This manuscript is a pre-print and has been submitted for publication in Quaternary Geochronology

Reducing variability in OSL rock surface dating profiles.

Joanne Elkadi [a,*], Georgina E. King [a], Benjamin Lehmann [b] and Frédéric Herman [a]

[a] *Institute of Earth Surface Dynamics, University of Lausanne, 1012 Lausanne, Switzerland*

b Laboratoire EDYTEM, Université Savoire Mont Blanc- CNRS, 73376 Le Bourget-du-Lac, France

**Corresponding author: joanne.elkadi@unil.ch*

Abstract

In recent years, rock surface dating has seen the emergence of a technique based on optically stimulated luminescence (OSL). This application translates the depth of OSL signal bleaching within a rock surface into an exposure age or erosion rate at 1-10^4 a timescales. Considerable effort has been undertaken to improve our understanding of OSL rock surface dating, yet a large amount of uncertainty associated with the method remains. Specifically, OSL profiles measured into rock surfaces can be highly scattered. Potential causes of this scatter could be lithological heterogeneity that modify bleaching rate throughout the rock, variability in surface erosion or experimental artefacts. Here, we report experiments that were conducted to explore whether experimental artefacts could contribute to the scatter in OSL profiles measured from rock surfaces exposed in Zermatt, Switzerland. This was done by varying the following parameters: (i) heating rate, (ii) isothermal holding time, (iii) luminescence signal detection filters, (iv) the sequential order of optical stimulations, and (v) core diameter. Our results indicate that sample temperature, for both preheating and stimulation, may exert a strong influence on the OSL profiles obtained. Thermal lag, i.e. the temporal offset between sample temperature and the instrument temperature, can be significant for rock slices if a heating rate of 5 °C s^{-1} is used and if rock slices are placed directly on the instrument carousel. To reduce this effect, our results suggest future studies place samples in metal cups, reduce the heating

rate and increase preheating and holding times prior to optical stimulation, to allow samples to heat at the desired rate and reach the required temperatures.

Keywords:

OSL surface exposure dating

Heating rate

Gorner glacier

Luminescence depth profiles

1. Introduction

Optically stimulated luminescence (OSL) dating is a trapped charge dating technique that measures the intensity of light emitted from a mineral (e.g. quartz or feldspar) following stimulation by light (Huntley et al., 1989; Aitken, 1998). The method is widely used and has traditionally been applied to the dating of sedimentary deposits (e.g. Rhodes, 2011), but has also recently shown a strong potential for rock surface dating applications (e.g. Sohbati et al., 2011; 2012a).

OSL rock surface dating hinges on the principle that the energy of photons emitted by the sun is sufficient to reset the luminescence signal in minerals at the surface of the Earth. This phenomenon is termed "bleaching". Research has shown that this bleaching effect decreases with depth into a rock surface (Habermann et al., 2000; Polikreti et al., 2002; 2003; Laskaris and Liritzis, 2011), due to attenuation of the photon flux, until it eventually becomes negligible. Studies have also suggested a link between exposure time and the depth of bleaching- where the longer a surface has been exposed to daylight, the deeper into the rock surface the luminescence signal is bleached (Habermann et al., 2000; Polikreti et al., 2002; Laskaris and Liritzis, 2011; Sohbati et al., 2011; 2012a; Lehmann et al., 2018; Gliganic et al., 2019). Thus, after calibration, the luminescence bleaching profile beneath a rock surface may be used to obtain information regarding the surface's exposure history. At present, OSL rock surface dating can be applied either to determine surface exposure (e.g. Lehmann et al., 2018) or surface burial (e.g. Simms et al., 2011; Jenkins et al., 2018).

A major advantage of OSL rock surface dating is that it complements cosmogenic nuclide surface exposure dating (e.g. using ^{10}Be, ^{14}C). For surfaces that have experienced minimal

erosion, the luminescence profiles with depth can provide exposure ages on time scales of 10^0-10^4 a, compared to cosmogenic nuclide dating which resolves time scales of the order 10^3-10^6 a. OSL rock surface dating has already been successfully used in a variety of different applications, including archaeological settings (e.g. Chapot et al., 2012; Liritzis and Vafiadou., 2015; Sohbati et al., 2015) as well as relative sea level (Simms et al., 2011; Simkins et al., 2013), paleo ice sheet (Simms et al., 2012; Jenkins et al., 2018) and Alpine glacier (Lehmann et al., 2018; 2019; 2020) reconstructions. On the other hand, for surfaces that have experienced considerable erosion which affects their apparent exposure age (e.g. Lehmann et al., 2019 showed that a 4 mm a^{-1} erosion rate over the last 344 years could alter an exposure age by 930%), OSL rock surface dating can be used to calculate erosion rates (Sohbati et al., 2018, Lehmann et al., 2019).

Despite significant advancements over the past years, luminescence-depth bleaching profiles are unfortunately often highly scattered and the cause of this scatter remains unexplained; potential sources include: (1) lithological variations within a rock surface that subsequently influence light penetration, (2) variability in surface erosion affecting the apparent bleaching depths in luminescence profiles or (3) experimental artefacts. Various studies investigating the effects of lithology (Meyer et al., 2018; Ou et al., 2018) and erosion (Sohbati et al., 2018; Lehmann et al., 2019) on luminescence profiles have been carried out, yet none have addressed the influence of experimental artefacts. In this study, we explore the latter point. To do this, we ran four experiments on bedrock samples collected from Zermatt, Switzerland, in which we varied several parameters from the measurement protocol.

2. Rock Surface Dating

2.1 Previous rock surface dating studies and their respective measurement parameters

Since its initial use in the dating of archaeological settings through the bleaching of thermoluminescence (TL) signals (e.g. Liritzis, 1994; Richards, 1994; Theocaris et al., 1997), rock surface dating has expanded to include a variety of applications, and shifted its focus to measuring Infrared Stimulated Luminescence (IRSL) and Optically Stimulated Luminescence (OSL) signals from feldspar and quartz, respectively.

Recent rock surface dating studies have predominantly focused on the measurement of IRSL and OSL signals from multi-mineral rock slices. Table 1 summarises these studies and emphasises the variations in protocol parameters, such as the heating conditions and the placement of slices on the carousel during measurement using Risø readers. This compilation does not include rock surface dating studies that involved the measurement of grains from mineral separates instead of whole slices (Chapot et al., 2012; Sohbati et al., 2012a; al Khasawneh et al., 2018; Gliganic et al., 2019).

2.2 Components involved in rock surface dating measurement protocols

As indicated in Table 1, during measurement slices can either be placed directly on a carousel or in stainless steel cups. This is usually dependent on the size and shape of the slices.

A standard measurement protocol for measuring the OSL signal of a rock slice follows that of the well-established SAR protocol (Murray and Wintle, 2000), and begins with a preheat

109 treatment where the slice is heated to an assigned temperature (e.g. 250°C) with no light
110 stimulation. This process removes short-lived and unwanted electrons that accumulate in traps
111 of low activation energy and are unstable at room temperature (e.g. Aitken, 1985; 1998; Murray
112 and Wintle, 2000). Once this temperature is attained, the sample is then held for a designated
113 amount of time - termed the preheat isothermal hold. It is assumed that all shallow electron
114 traps have been emptied by the end of the preheat (e.g. Murray and Wintle, 2000). The heating
115 rate and isothermal holding time for a preheat can vary and, in dating studies, it is imperative
116 to choose appropriate values as incorrect values may cause inefficient heating of the sample
117 due to rocks' low thermal diffusivity (0.6 to 1.9 $mm^2 s^{-1}$; Drury, 1987). Any remaining electrons
118 can potentially contribute to subsequent luminescence measurements (Aitken, 1998). If
119 thermal treatments are not reproducible between measurement cycles, and the degree of
120 thermal lag varies between slices, then this inter-slice heating variability could result in scatter
121 in the data. We are able to monitor the thermal treatment experienced by the sample by
122 recording the TL signal emitted during the preheat in a sequence.
123
124 Following the preheat, slices are optically stimulated to measure their OSL signal. To do this,
125 the sample is heated to a fixed temperature and held for a specified time duration prior to
126 switching on the diodes. Samples are measured at elevated temperature to ensure that unstable
127 traps potentially populated by thermal transfer during the preheat do not contribute to the
128 measured OSL signal. As with a preheat, the heating rate and pre-stimulation isothermal hold
129 can be altered to ensure that the samples reach the required temperature in a uniform manner.
130 If a sample is heated too rapidly, or not held at temperature for a sufficient amount of time, we
131 risk producing misleading OSL results due to inter-slice heating variability mentioned
132 previously. As a result, scatter would be observed in the data, but the effect of this can be
133 minimised by choosing the correct measurement parameters. Thermal assistance is particularly

key for the measurement of feldspar IRSL, emphasising the need for accurate and reproducible thermal measurement conditions (e.g. Hütt et al., 1988).

Most modern luminescence readers are semi-automated, and the different thermal and optical treatments and irradiations of a given measurement sequence are programmed for the instrument using software such as Sequence Editor. Whilst we program a desired final temperature for any thermal treatment, it is generally difficult to monitor the exact heating rate and temperature that the sample experiences during measurement. In contrast, it is possible to predict when trapped charge will be evicted from a mineral using the kinetic parameters that describe a particular luminescence signal's thermal stability. Generally, lower heating rates result in the equivalent trapped charge being evicted at lower temperatures and the converse is also true (e.g. Schmidt et al., 2018). For example, quartz has a well characterised TL peak at ~100 °C, termed the '110 °C peak', when heated at 5 °C s^{-1} (Bailey, 2001), however the peak position varies depending on the heating rate of the sample. We can use the position of the 110 °C peak in a TL curve from a preheat to approximate a sample's thermal pretreatment (Duller et al., 2020), and in particular a sample's heating rate.

Citation	Dating application	Core diameter (mm)	Target mineral	Detection filter	Preheat		Stimulation		Slices resting in cups or directly on carousel?
					Heating rate (°C s^{-1})	Isothermal hold (s)	Heating rate (°C s^{-1})	Isothermal hold (s)	
Feathers et al., 2019	Burial	10	Fsp	(d)	-				Cups
Freisleben et al., 2015	Burial	~10	Fsp	(a)	-				-
Jenkins et al., 2018	Burial	~8	Fsp	(b)	1	100	1	100	Cups
Lehmann et al., 2018	Exposure	~10	Fsp	(d)	5	60	5	5	Carousel
Lehmann et al., 2019	Exposure	~10	Fsp	(d)	5	60	5	5	Carousel
Liu et al., 2019	Exposure	~10	Fsp	(a)	-	100	-	30	-
Luo et al., 2018	Exposure	~10	Fsp	(d)	-	100	5	30	-
Meyer et al., 2018	Exposure	~8	Qtz and Fsp	(e) for Qtz (c) for Fsp	5	-	5	14	Carousel
Ou et al., 2018	Exposure	~7	Fsp	(b)	1	100	1	100	Cups
Rades et al., 2018	Burial	~10	Fsp	(c)	-	100	-	-	-
Sohbati et al., 2011	Exposure	~10	Fsp	(c)	-	60	-	30	Carousel
Sohbati et al., 2012b	Burial	10	Qtz	(f)	5	100	5	100	Carousel
Sohbati et al., 2015	Burial	~10	Fsp	(a)	5	60	5	30	Carousel
Sohbati et al., 2018	Exposure	10	Fsp	(a)	-	100	-	30	-
Souza et al., 2019	Burial	~10	Fsp	(a)	-	100	-	30	Carousel

Table 1: Compilation of previous rock surface dating studies. Fsp and Qtz denote feldspar and quartz respectively. With regards to the filters, (a) = Schott BG-39/Corning 7-59 (2 and 4 mm respectively), (b) = Schott BG-39/Corning 7-59 (2 mm each), (c) = Schott BG-39/ Corning 7-59 (unspecified thickness), (d) = Schott BG3 and BG39, (e) = 7.5 mm Hoya U-340 and (f) = ~ 7 mm Hoya U-340. The cups are made of stainless steel. (-) is for when the information was unspecified.

3. Methodology

3.1 Sample preparation

The two samples mentioned in this study, GG17-05-01 and GG18-05-01, are both schists from the same sample site. They were collected as part of a suite of samples in October 2018 from the mountainside adjacent to the Gorner glacier, located close to the village of Zermatt, Switzerland. Sample GG17-05-01 was extracted from a surface with an unknown exposure age, and GG18-05-01 was collected from a surface that had been exposed during sampling of GG17-05-01 the previous year, so has a well-constrained exposure age of 342 days.

The samples were taken from bedrock using a combination of a hammer, chisel and Husqvarna K760 power cutter with a diamond blade. They were collected as ≈15 cm x 15 cm x 10 cm dimension blocks and immediately placed into black, light obstructing bags. In the laboratory, the blocks were then drilled using a water-cooled Husqvarna DM220 drill to extract cores of either 5 mm or 10 mm diameter. Generally, smaller diameter cores of this lithology break more easily during drilling, and extracting intact cores can be tedious and time consuming without the guarantee of a successful result. It was therefore necessary to drill multiple cores for every core successfully extracted. To avoid any potential signal resetting that may have occurred during fieldwork, the cores were drilled in the centre of the block and as far from the block edge as possible. These cores were then cut into slices using a BUEHLER Isomet low speed saw, mounted with a 0.3 mm thick diamond blade in the presence of a lubricant. The exact thickness of each slice was measured using a TESA Digitcal caliper, and the final average thicknesses ranged from 0.32 to 1.11 mm. All laboratory work was done under subdued red-light conditions.

179

180 *3.2 Measurement protocols*

181

182 To investigate the influence of experimental artefacts on the scatter in luminescence profiles,
183 we focused on changing the following parameters: (i) heating rate, (ii) preheat and pre-
184 stimulation isothermal holding times, (iii) luminescence signal detection filters, (iv) order of
185 optical stimulations, and (v) core diameter. This was done across four experiments - A, B, C
186 and D - and each experiment contained three parts (Part i, ii and iii). A summary of the different
187 experimental protocols can be found in Table 2, and these are elaborated on in Tables S1-S4
188 in the Supplementary Material.

189

190 All experiments were performed on three 5 mm diameter slices and three 10 mm diameter
191 slices from Sample GG18-05-01. The slices had been depleted of their natural signal using
192 measurement protocol Ai, with the 5 mm diameter slices placed in stainless steel cups and the
193 10 mm diameter slices resting directly on the carousel. The average thickness of the slices used
194 in these experiments ranges from 0.59 to 0.62 mm for the 10 mm diameter slices and from 0.57
195 to 0.58 mm for the 5 mm diameter slices. For both diameter types, the slices were measured
196 without any additional mineral separation, and so were composed of an amalgamation of
197 several minerals. Due to this, the measurement protocols included $IRSL_{50}$, OSL_{125} and post-IR
198 $IRSL_{225}$ stimulations, with the optimum sequence order and filter combinations explored as an
199 aspect of the experiments in this study. The recent instrumentation development of a DASH
200 reader head allows for filter combinations to be changed throughout a measurement sequence
201 (Lapp et al., 2015) and tailored to the target mineral's emission. Measuring multiple
202 luminescence signals, and thus different minerals and traps with varying bleaching
203 characteristics, allows us to obtain a maximum amount of information from samples. However,

as feldspar is also responsive to blue light stimulation, it is unlikely that we are able to isolate a pure quartz signal. Nevertheless, combining IRSL and OSL luminescence signals to extract information from samples has been successfully investigated previously for both sediments and rock slices (e.g. Reimann et al., 2015, Meyer et al., 2018). With the exception of natural luminescence signals, measurements were made in response to a given regenerative dose of 51.75 Gy and a test dose of 51.75 Gy. The samples were stimulated for 200 s and the luminescence signals for all measurements were integrated over the first 10.8 s of stimulation, with a background signal taken from the final 57.7 s of stimulation.

Measurements of the natural signal, for the reconstruction of luminescence depth profiles, were made on several cores from samples GG17-05-01 and GG18-05-01. Experimental protocol Ai was initially used on three cores, each with a diameter of 10 mm, from sample GG18-05-01 to generate preliminary results. After analysing the results using this protocol, it was decided to undertake the experiments in this study and subsequently three cores from the same sample were taken and measured using protocol Biii, using a combination of 5 mm diameter slices and broken fragments from 10 mm diameter slices. Each core was composed of 24 slices, with the protocol Ai slices resting directly on the carousel and protocol Biii slices sat in stainless steel cups on the carousel. Slices from these cores were subsequently used in the experiments discussed above. Both protocols were also used to measure cores from GG17-05-01, for the purpose of exposure age calculations which are elaborated on in Section 6.1.

3.3 Measurements

All experimental measurements were carried out on a Risø TL/OSL-DA-20 luminescence reader (Bøtter-Jensen et al., 2010), ID Number 396, equipped with a DASH head (Lapp et al.,

2015) and a $^{90}Sr/^{90}Y$ beta source at the University of Lausanne, Switzerland. The reader had a dose rate of 0.207 ± 0.005 Gy s^{-1} calibrated to gamma irradiated quartz slices resting on the measurement carousel and yields a dose rate 11.4% lower than for coarse grained quartz. Its instrument reproducibility is ~1.8%. The measurements of the natural signal from samples GG17-05-01 and GG18-05-01 were carried out using a combination of the aforementioned Risø reader, in addition to two Risø TL/OSL-DA-20 luminescence readers (Bøtter-Jensen et al., 2010).

All stimulations done at a temperature greater than 200 °C were carried out under a nitrogen atmosphere.

3.4 Instrument behaviour

Independent thermocouple measurements were performed to assess the behaviour of the TL/OSL-DA-20 luminescence reader ID Number 396 (Bøtter-Jensen et al., 2010) used for the experiments in this study. Various temperatures were prescribed to the reader using the Sequence Control software and, using a thermocouple tip soldered to a stainless steel measurement cup, the corresponding actual thermocouple temperature was measured using a multimeter. The results are shown in Table 3. Across the range of temperatures used in the experimental measurement protocols of this study (Table 2), we see a maximum deviation of 8 °C between the measured and prescribed temperatures for the temperature range up to 300 °C, thus confirming the reader's sample holder is reaching temperature within this tolerance.

Prescribed temperature (°C)	50	75	100	125	150	175	200	225	250	300
Measured temperature (°C)	50	76	99	120	145	170	192	221	245	295

252 **Table 3:** Results from independent thermocouple measurements on the Risø reader to confirm
253 instrument behaviour.

254 *3.5 Modelling TL curves*

255

256 As mentioned in Section 2.2, for the Risø TL/OSL-DA-20 instruments used in these
257 experiments, no measurement of actual sample temperature is possible once a sequence is
258 launched. Since the rock slices were composed of a mixture of minerals, including quartz, the
259 general kinetic model of quartz from Bailey (2001) implemented in the R-package
260 'RLumModel' (Friedrich et al., 2016) was used to predict the position of the 110 °C peak in
261 quartz as a function of the prescribed heating rate. The model has an electron trap depth of 0.97
262 eV and a frequency factor of 5×10^{12} s^{-1}. The 110 °C peak was chosen as it is believed to follow
263 a first order kinetic behaviour (e.g. Pagonis et al., 2003) and is ubiquitous in quartz samples.
264 Once the theoretical 110 °C peak position was calculated using the chosen model, it could then
265 be compared to the experimental peak positions generated by the rock slices during
266 measurement to provide information on their heating.

267

268 # 4. Results

269

270 *4.1 Natural samples*

271

272 The resultant luminescence profiles with depth for the natural signal of sample GG18-05-01
273 measured using protocols Ai and Biii, along with their corresponding model plots and chi-
274 square goodness of fit (χ^2) values, are shown in Figure 1. Protocol Ai was applied to 10 mm
275 diameter slices resting directly on the carousel and used U340 filters for every stimulation,
276 whereas protocol Biii was applied to a combination of 5 mm diameter slices and broken

277 fragments of 10 mm diameter slices resting in stainless steel cups on the carousel, and used a
278 combination of U340 and BG39+BG3 filters depending on the target mineral (see Table 2).
279 The $IRSL_{50}$ absolute signal counts from slices measured using protocol Biii were, on average,
280 one or two orders of magnitude lower than their corresponding measurements using protocol
281 Ai. In each case, the luminescence signal has been normalised to the average value of the
282 plateau, which is determined qualitatively once the luminescence signals are no longer
283 increasing with depth. For the noisy post-IR $IRSL_{225}$ Experiment Ai profile, normalisation was
284 done by taking an average of all the measurement points. By visually analysing the depth
285 profiles across all three signals, it is immediately clear that the measurements made using
286 protocol Biii generate depth profiles that are much less scattered than those measured using
287 protocol Ai, particularly for the feldspar IRSL signals. This is further confirmed by the χ^2
288 values, which improve across all three signals for protocol Biii - even in the case of the OSL_{125}
289 signal which initially visually does not appear to show any reduction in scatter.
290
291 Figure 2 displays the TL plots generated during the natural (L_n) and test dose (T_n) measurements
292 of the GG18-05-01 natural signal slices in Figure 1. For both the L_n and T_n measurements, the
293 TL curves generated using the Experiment Ai protocol exhibit large differences in their peak
294 positions. The T_n curves show less variation than the L_n curves, with peak signal intensities
295 occurring closer to when the heating plate attains its maximum temperature, whereas the L_n
296 curves peak at, or later than, the heating plate reaching its maximum temperature. In contrast,
297 the TL curves for Experiment Biii reveal smaller discrepancies in their peak positions for both
298 the L_n and T_n measurements. Overall the Experiment Biii TL curves peak earlier than their
299 Experiment Ai counterparts for both the L_n and T_n measurements.
300

The T_n plots for both experimental protocols have been overlain with theoretical quartz TL curves generated using the general kinetic model of quartz (Bailey, 2001) implemented in the R-package 'RLumModel' (Friedrich et al., 2016, Section 3.5) by prescribing each protocol's heating rate. As expected, the quartz 110 °C peak is absent from the L_n plots for both protocols, as it is a short-lived peak with a half-life of ~70 min (cf. Schmidt et al., 2018). We have thus not plotted the theoretical quartz TL curves on the L_n plots. The inconsistency in 110 °C peak positions between the measured and theoretical TL curves is greatly reduced in the plots of Experiment Biii when compared to those of Experiment Ai. Furthermore, the Figure 2 T_n plots measured using Experiment Biii have both the 110 °C peak, associated with quartz, and a low temperature peak at ~140 °C, commonly found in feldspars (e.g. Duller and Botter-Jensen, 1993), present as opposed to the T_n plots generated using Experiment Ai where they are both absent.

313

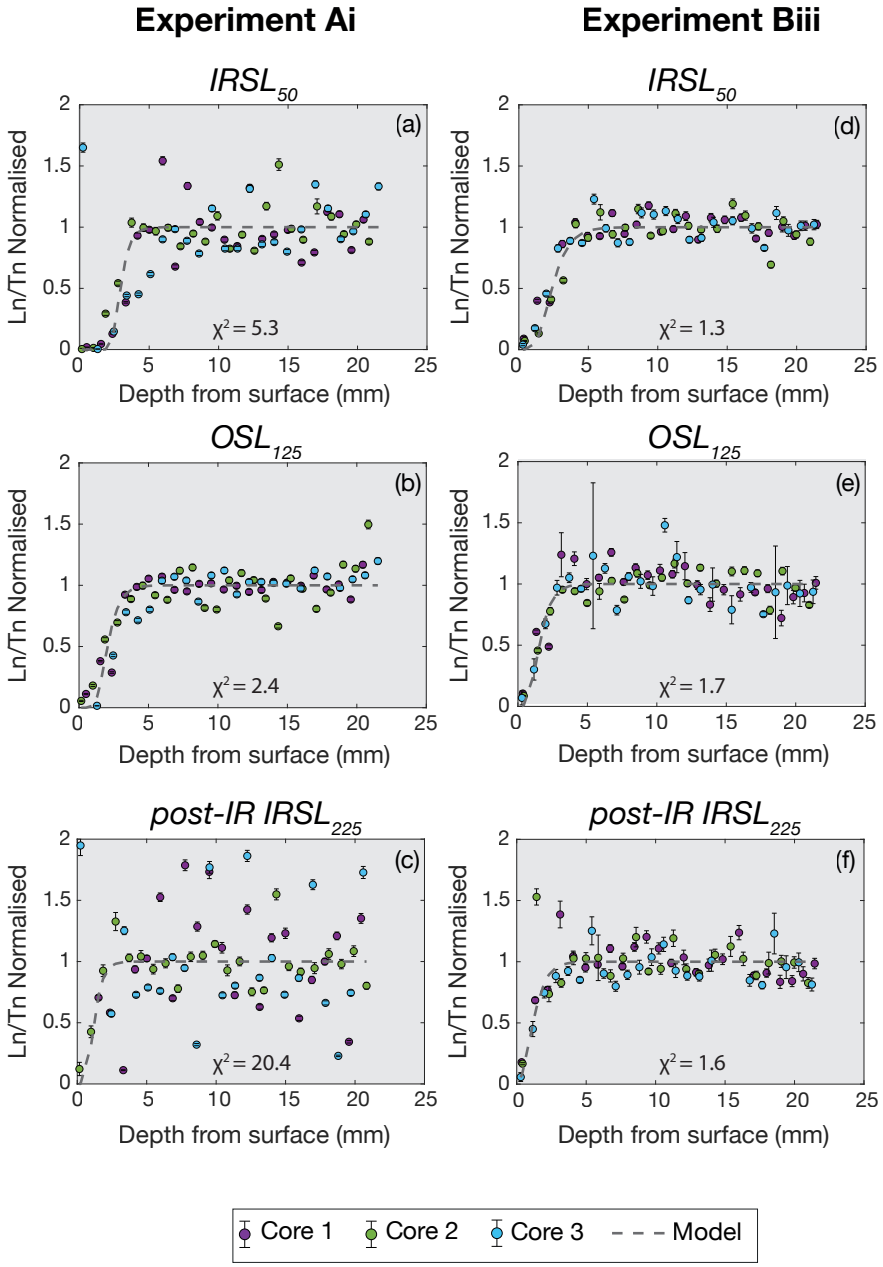

Figure 1: Luminescence depth profiles generated for the natural $IRSL_{50}$, OSL_{125} and post-IR $IRSL_{225}$ signals from sample GG18-05-01, with their corresponding modelled plots and χ^2 values. Each profile is constructed using three separate cores (denoted by the three colours) and each point is a luminescence measurement from a slice at that particular depth. The luminescence signal is normalised in each case to the average value of the plateau, which is determined qualitatively once the luminescence signals are no longer increasing with depth. The errors are taken directly from the Analyst programme, and are derived from the square root of the luminescence counts. Experiment Ai (a-c) had 10 mm diameter slices resting directly on the carousel and used a heating rate of 5 °C s^{-1} while Experiment Biii (d-f) had 5 mm diameter slices and broken fragments sat in stainless steel cups on the carousel and a heating rate of 1 °C s^{-1}.

314

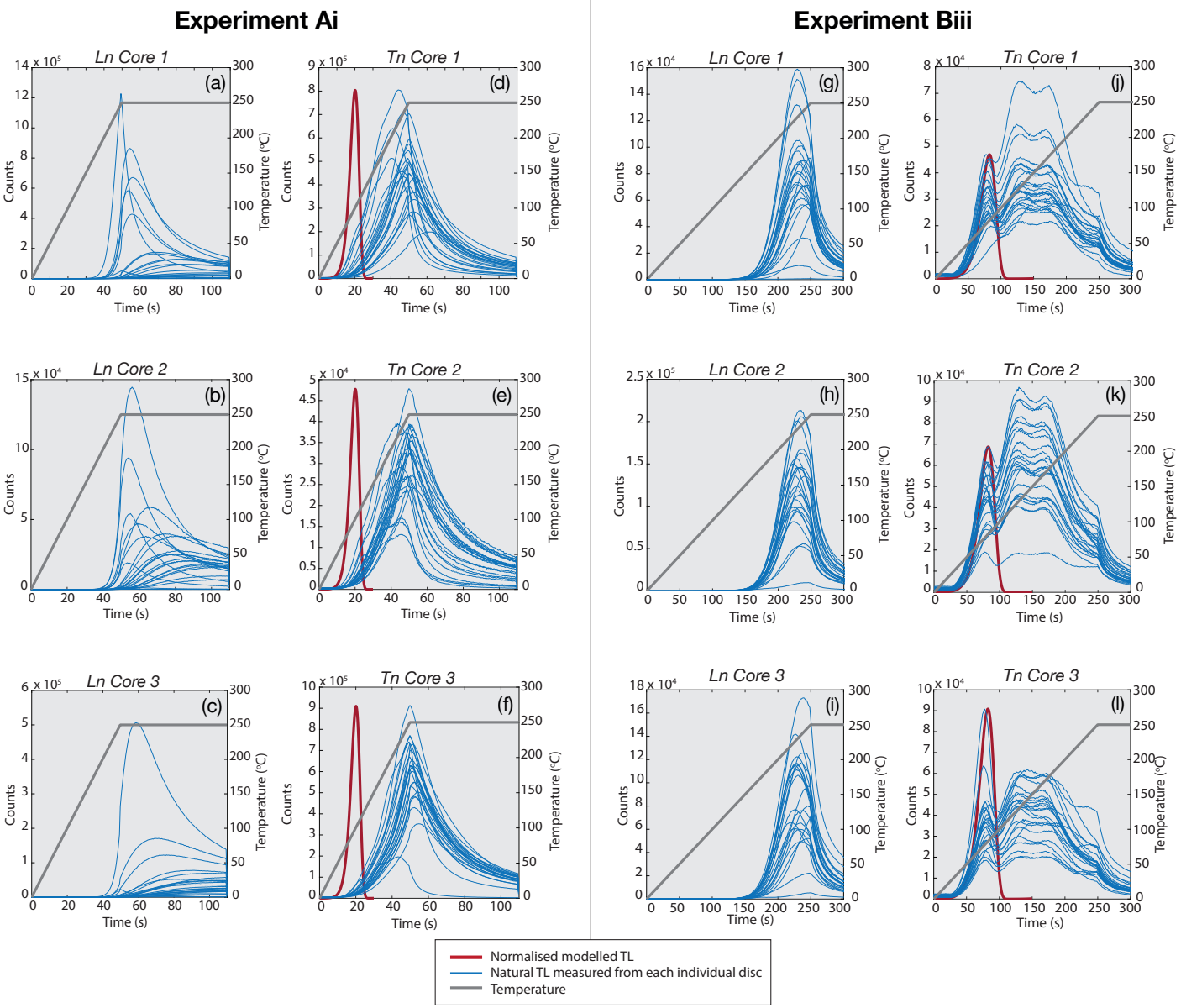

Figure 2: TL curves produced during the L_n and T_n measurements of the natural signal in sample GG18-05-01. Each core was up made of 24 slices. Experiment Ai (a-f) had 10 mm diameter slices resting directly on the carousel and Experiment Biii (g-l) had 5 mm diameter slices and broken fragments sat in stainless steel cups on the carousel. The theoretical quartz curves (red) were generated using the general kinetic quartz model (Bailey, 2001) implemented using the R-package 'RLumModel' (Friedrich et al., 2016) by prescribing each experimental protocol's respective heating rate. The intensity of the theoretical TL curves has been normalised to the maximum experimental peak intensity for Experiment Ai and their corresponding experimental 110 °C peaks for Experiment Biii.

315 *4.2 Experimental protocols*

316

317 *4.2.1 Signal properties and reproducibility*

318

319 To assess reproducibility for all four experiments and three signals, each slice was measured
320 five times following lab irradiation, and the relative standard deviation (RSD) of the L_x signal
321 measurements was calculated. All three signals were reproducible with RSD of <10 % for the
322 $IRSL_{50}$, OSL_{125}, and post-IR $IRSL_{225}$ signals for 94 % of measurements. Furthermore, for all
323 slices, the luminescence signals were checked for two acceptance criteria: (1) maximum error
324 of test dose signal (T_n) of <15% and (2) T_n greater than 3σ above the background signal. Across
325 the four experiments, all slices passed the screening for the three stimulation signals except for
326 one 10 mm diameter slice which failed both tests for the post-IR $IRSL_{225}$ stimulation in
327 Experiment Aiii and all parts of Experiment B. The slice's data from these experiments has
328 been excluded from any further analysis.

329

330 *4.2.2 Signal intensity*

331

332 One aspect of the experiments involved comparing the use of different detection filters during
333 IRSL measurements, particularly the effect of using a U340 filter as opposed to the blue filter
334 pack (BG39 + BG3). To do this, the intensity of the Lx signal, for both $IRSL_{50}$ and post-IR
335 $IRSL_{225}$, from parts (i) and (ii) of each experiment were compared. This assessment is possible
336 because these two sections within each experiment have the same measurement conditions, in
337 terms of the sequence order and heating parameters used. The only difference between these
338 two parts lies in the detection filters used for the IRSL measurements- part (i) uses U340 filters
339 whereas part (ii) the BG39+BG3 blue filter pack. Part (iii) of each experiment was excluded

from analysis as it includes a change in the order of stimulation which therefore doesn't allow for a clear comparison. Examples of the comparison results from Experiments B and D can be found in Tables S5 and S6. For both the $IRSL_{50}$ and post-IR $IRSL_{225}$ signals, across both slice sizes, the average Lx intensities from part (i) were either of equal magnitude or one magnitude lower than the results from part (ii).

Another objective of this study entailed investigating the order of light stimulation modes, specifically that of the OSL_{125} and post-IR $IRSL_{225}$ signals. Parts (i) and (ii) of each experiment have the OSL_{125} stimulation occurring prior to that of the post-IR $IRSL_{225}$ whereas in part (iii), the order of these two stimulations was reversed. To understand the effect of this, the intensity of the luminescence signal for each stimulation was compared across the experiments. Figure 3 shows an example of the results, taken from Experiment B. Since there was high reproducibility across the cycles (Section 4.2.1), for the remainder of this section, all signal intensity values are quoted as an average of all five cycles. In the 10 mm core results, the OSL_{125} and post-IR $IRSL_{225}$ signals, using a sequence order whereby the OSL_{125} stimulation occurs prior to the post-IR $IRSL_{225}$ (Experiment Bii), have signal intensity values of 12.5×10^4 and 3.4×10^4 counts/second (cts s^{-1}), respectively. Once the order is reversed in Experiment Biii, there is a 73.9 % increase in the post-IR $IRSL_{225}$ signal intensity to 5.9×10^4 cts s^{-1} at the expense of the OSL_{125} signal which is reduced by 17.6 % to 10.3×10^4 cts s^{-1}. A similar pattern is observed for the 5 mm cores once the sequence order is reversed, but with a smaller magnitude of change. The post-IR $IRSL_{225}$ signal increases by 50.0 % from 1.0×10^4 to 1.5×10^4 cts s^{-1}, alongside a 19.0 % decrease in OSL_{125} signal intensity from 4.2×10^4 to 3.4×10^4 cts s^{-1}.

Stimulation	Filter	Heating rate ($^{o}C\ s^{-1}$)	Isothermal hold (s)	Signal	Target mineral
Regenerative dose 51.75 Gy					
Preheat at 250°C	U340[i]/ BG39 + BG3[ii,iii]	5[A, D]/1[B,C]	60[A,C]/100[B,D]		
IRSL at 50°C	U340[i]/ BG39 + BG3[ii,iii]	5[A,D]/1[B,C]	5[A,C]/100[B,D]	$IRSL_{50}$ L_x	Feldspar
OSL at 125°C[i,ii]/ IRSL at 225°C[iii]	U340[i,ii]/ BG39 + BG3[iii]	5[A,D]/1[B,C]	5[A,C]/100[B,D]	OSL_{125} L_x	Quartz[i,ii]/ Feldspar[iii]
IRSL at 225°C[i,ii]/ OSL at 125°C[iii]	U340[i,iii]/ BG39 + BG3[ii]	5[A,D]/1[B,C]	5[A,C]/100[B,D]	post-IR $IRSL_{225}$ L_x	Feldspar[i,ii]/ Quartz[iii]
Test dose 51.75 Gy					
Preheat at 250°C	U340[i]/ BG39 + BG3[ii,iii]	5[A,D]/1[B,C]	60[A,C]/100[B,D]		
IRSL at 50°C	U340[i]/ BG39 + BG3[ii,iii]	5[A,D]/1[B,C]	5[A,C]/100[B,D]	$IRSL_{50}$ T_x	Feldspar
OSL at 125°C[i,ii]/ IRSL at 225°C[iii]	U340[i,ii]/ BG39 + BG3[iii]	5[A,D]/1[B,C]	5[A,C]/100[B,D]	OSL_{125} T_x	Quartz[i,ii]/ Feldspar[iii]
IRSL at 225°C[i,ii]/ OSL at 125°C[iii]	U340[i,iii]/ BG39 + BG3[ii]	5[A,D]/1[B,C]	5[A,C]/100[B,D]	post-IR $IRSL_{225}$ T_x	Feldspar[i,ii]/ Quartz[iii]
Repeat 5 times					

Table 2: Overview of experimental protocols tested in this study. A, B, C and D denote the different experiments and [i, ii, iii] represents the different parts within each experiment (i.e. there was Experiment Ai, Aii, Aiii and the same for Experiments B, C and D). A 7.5 mm U340 filter was used.

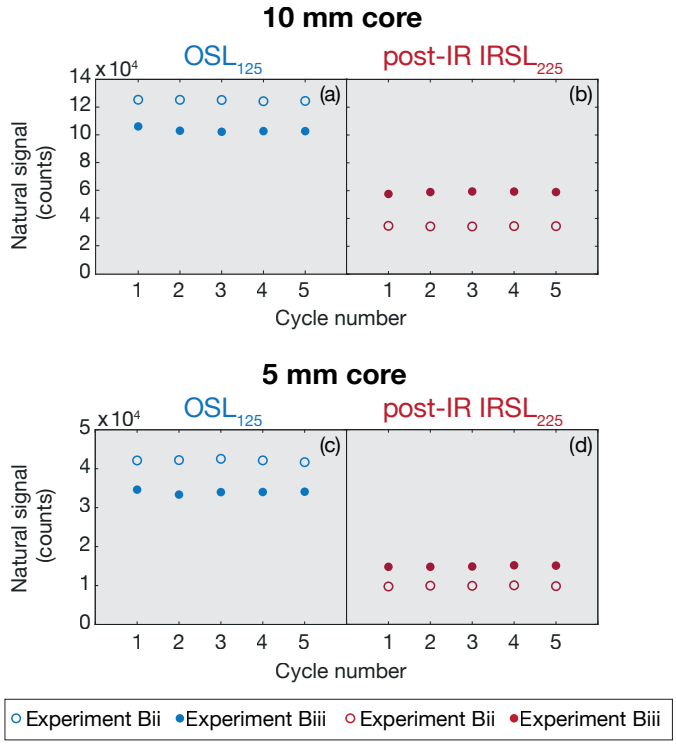

Figure 3: Comparison of OSL_{125} (blue) and post-IR $IRSL_{225}$ (red) natural signal counts from Experiments Bii and Biii to investigate the influence of varying the order of light stimulation. The slices were heated at a rate of 1°C s^{-1}, and each protocol was run five times on each individual slice (termed cycles in the figure). (a-b) are measured from slices sat directly on the carousel and (c-d) are results for slices resting within stainless steel cups on the carousel. Open circles represent Experiment Bii, which has the OSL_{125} stimulation prior to the post-IR $IRSL_{225}$ stimulation. Closed circles, for Experiment Biii, has these stimulations reversed with the post-IR $IRSL_{225}$ stimulation occurring before that of the OSL_{125}.

379 *4.2.3 TL curves*

380

381 By recording the TL signal emitted during the preheat in a sequence, we are able to glean some
382 information on the thermal treatment received by the sample. As shown in Table 2, prior to
383 stimulation each slice was subjected to a 250 °C preheat. Across the four experiments, the
384 heating rate and isothermal hold of the preheat were varied and examples of the resulting TL
385 curves from part (iii) of each experiment are illustrated in Figure 4.

386

For all four experiments, a consistent pattern emerges in both the TL curve peak positions and shapes when comparing the results from 10 mm diameter slices with those of 5 mm diameter slices. Within each experiment specifically, under the same measurement conditions, the TL of the 5 mm diameter slices peaks earlier than the 10 mm diameter slices. The TL curves of 5 mm diameter slices also have more of their TL curves emerging prior to the heating plate attaining its maximum temperature, when compared to their 10 mm slices diameter counterparts. In addition, the shape of the TL curves for the 5 mm diameter slices is different with more pronounced peaks and troughs than that of the 10 mm diameter slices. This difference in shape is not solely observed within specific experiments, but also across experiments. For example, there is a distinct difference in shape when looking at the 10 mm diameter slice TL curves in Experiments Aiii (Fig. 4a) and Diii (Fig. 4d) as opposed to a 10 mm diameter slice result in Experiment Biii (Fig. 4b) or Experiment Ciii (Fig. 4c). The slices heated using a lower heating rate of 1 °C s^{-1} (Fig. 4b and 4c, Experiments Biii and Ciii) have a more pronounced expression of the low temperature peak when compared to the slices subjected to a higher heating rate of 5 °C s^{-1} (Fig. 4a and 4d, Experiments Aiii and Diii) where this low temperature peak is either missing or merged with the higher temperature peak. The 10 mm diameter slices, heated at 1 °C s^{-1} rate, also had their peaks slightly shifted away from the maximum temperature, but not to the extent of the 5 mm diameter slices.

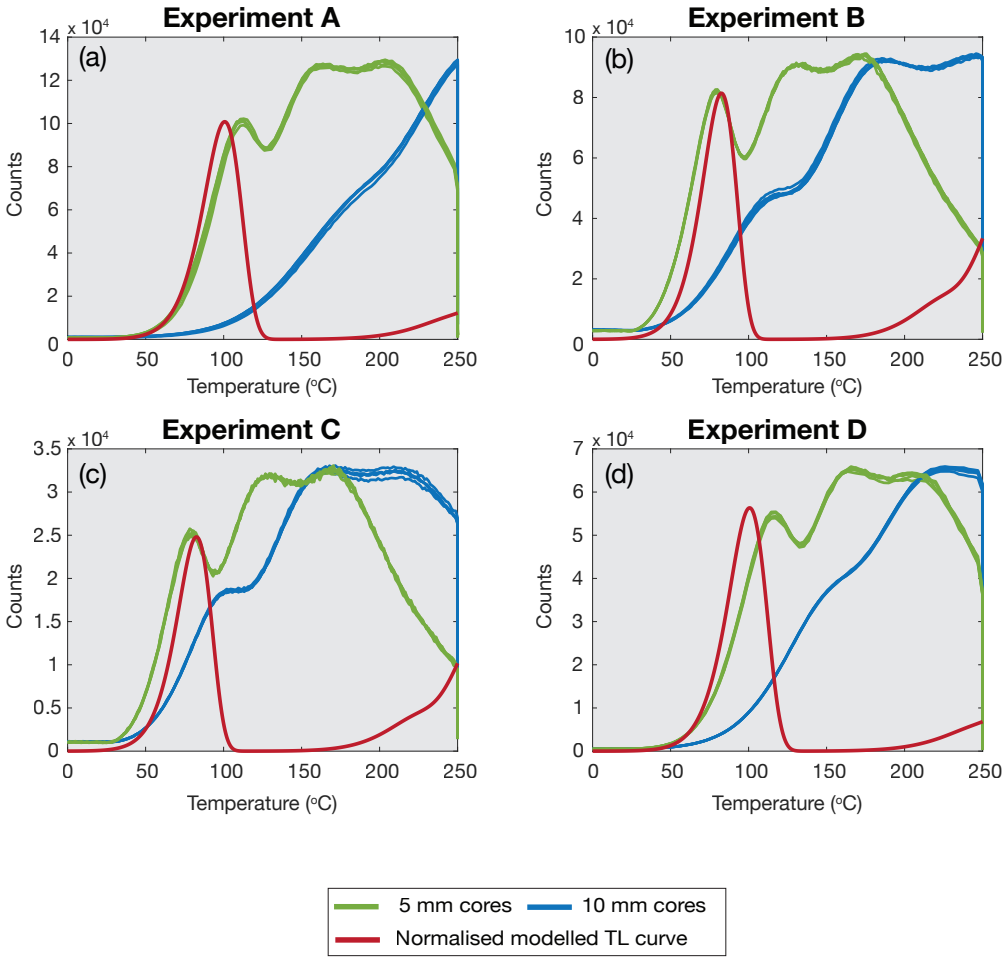

Figure 4: Theoretical quartz TL curves superimposed onto experimental TL curves from part (iii) of each experiment in this study. The theoretical quartz curves (red) were generated using the general kinetic quartz model (Bailey, 2001) implemented using the R-package 'RLumModel' (Friedrich et al., 2016) by prescribing each experiment's respective heating rate. The 10 mm diameter slices (blue) were resting directly on the carousel while the 5 mm diameter slices (green) sat in stainless steel cups on the carousel. The slices were heated to 250 °C, for Experiments A and D the heating rate was 5 °C s^{-1} whereas B and C were heated at a rate of 1 °C s^{-1}, and each slice was measured five times. The intensity of the theoretical TL curves has been normalised to their corresponding experimental 5 mm diameter 110 °C peaks. The intensity of the 10 mm diameter TL curves has also been normalised to their corresponding 5 mm diameter TL curves.

405

406

407

408 *4.2.4 Kinetic modelling*

409

410 Modelled quartz TL curves are used to show the theoretical 110 °C peak position in the absence
411 of any thermal lag, for a specific heating rate. By comparing these theoretical TL curves to
412 experimentally generated TL curves, we are able to quantitavely evaluate the degree of thermal
413 lag experienced by a sample. In this case however, as we are working with a signal resultant
414 from an amalgamation of minerals and not pure quartz, isolating the exact positions of the 110
415 °C peak from the 10 mm diameter slice TL curves that our experiments had produced is
416 difficult, as the overall TL curve is likely composed of several smaller sub-peaks. Therefore,
417 the experimental 110 °C peak positions were visually estimated. Theoretical quartz TL curves
418 were generated using the general kinetic model of quartz (Bailey, 2001) implemented in the R-
419 package 'RLumModel' (Friedrich et al., 2016; Section 3.5) by prescribing each experiment's
420 respective heating rate. Superimposing the modelled curves on the experimental TL curves
421 (Fig. 4) reveals a pronounced mismatch in the theoretical and experimental positions of the 110
422 °C peak in results from Experiments A and D (5 °C s^{-1} heating rate) as opposed to the results
423 from Experiments B and C (1 °C s^{-1} heating rate). The discrepancy in theoretical and
424 experimental peak positions is reduced further when comparing the 5 mm diameter slice TL
425 curves to their 10 mm diameter slice counterparts within each individual experiment - even for
426 the 10 mm diameter slice experiments with low heating rates. This is emphasised in Table 4,
427 which states the maximum peak position values for the 110 °C theoretical and experimental
428 peaks in each experiment. Across the five cycles for both the 10 mm and 5 mm diameter slices
429 in all four experiments, the peak positions were reproducible with a RSD < 1.5%.

430

431

432

		110 °C peak positions		
		10 mm diameter slice	5 mm diameter slice	Theoretical
		Experimental	Experimental	
Experiment	Heating rate (°C s^{-1})	Temperature (°C)	Temperature (°C)	Temperature (°C)
A	5	~185.8	112.8	100.5
B	1	~115.2	78.6	82.6
C	1	100.8	78.4	82.6
D	5	~159.6	117.5	100.5

Table 4: Comparison of experimental and theoretical 110 °C peak positions across all four experiments for the two different slice diameters. The peak positions are determined from peak maximum rather than peak fitting. The theoretical peak positions were calculated using the general kinetic model of quartz (Bailey, 2001) implemented in the R-package 'RLumModel' (Friedrich et al., 2016) by prescribing the heating rates for each experiment. For the Experimental 10 mm slice diameter results from Experiment A, B and D, the peak positions are approximate values because there is not a clear peak present but instead a shoulder (Fig. 4).

Additionally, we attempted to calculate kinetic parameters for the trap giving rise to the 110 °C peak for these samples, following the isothermal decay method outlined in Schmidt et al. (2018), but were unfortunately unable to generate realistic values due to feldspar contamination.

4.2.5 Luminescence decay curves

Figure 5 shows examples of post-IR $IRSL_{225}$ decay curves for 10 mm and 5 mm diameter slices across all four experiments. There is a clear difference between results from the two diameters. For all four experiments, the 10 mm diameter slice luminescence curves continue to rise even once the diodes have been switched on, and only peak after ~40 s of stimulation. In contrast, the 5 mm diameter slice decay curves have the characteristic luminescence decay shape

452 associated with a depleting electron trap. This discrepancy in decay is not observed in the decay
453 curves from $IRSL_{50}$ and OSL_{125} stimulations, which show typical luminescence decay curves
454 (data not shown).
455

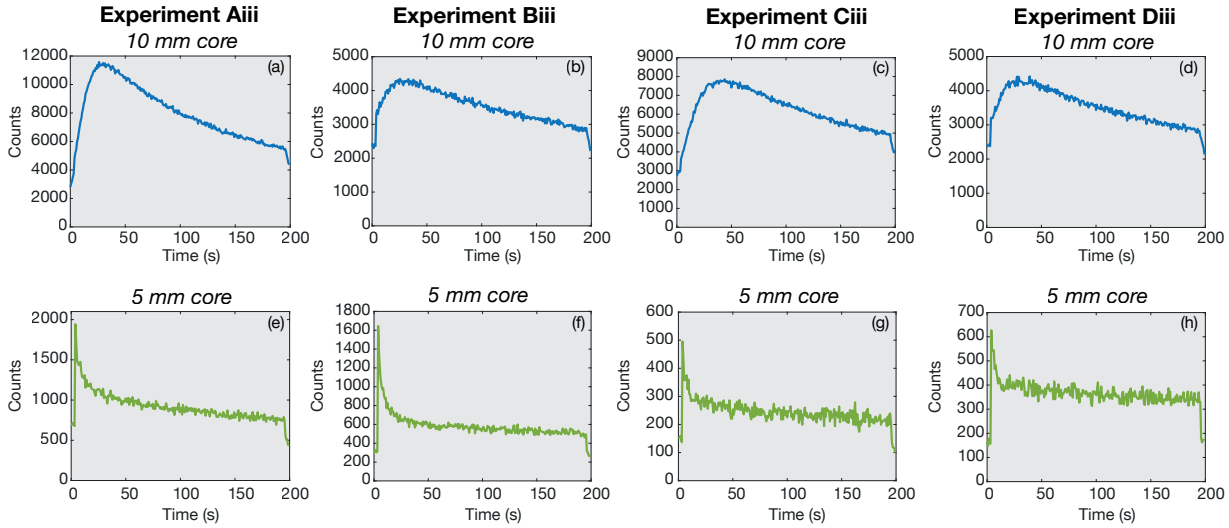

Figure 5: Post-IR $IRSL_{225}$ luminescence decay curves for 10 mm diameter slices (a-d) and 5 mm diameter slices (e-h) across all four experiments. The 10 mm diameter slices were resting directly on the carousel during measurement while the 5 mm diameter slices were in stainless steel cups. All four were subjected to protocols which had the post-IR $IRSL_{225}$ stimulation occurring after the $IRSL_{50}$ but prior to the OSL_{125} stimulations.

456 *4.2.6 Slice diameter*
457
458 We decided to investigate the importance of slice diameter on the luminescence profiles
459 generated. To do this, luminescence profiles with depth for Sample GG17-05-01 were
460 produced using two different core diameters, but with all slices resting in stainless steel cups
461 during measurement. One profile was from 5 mm diameter slices, and the other from what
462 were initially 10 mm diameter slices but had been broken into smaller fragments to fit inside
463 the stainless steel cups. The fragments had approximate surface areas of 25 mm^2. The results
464 are shown in Figure 6 and we see that the two luminescence profiles generated are very similar,

465 implying that for this lithology slice diameter is inconsequential to the results, and that the
466 predominant factor is the placement of all rock slices in stainless steel cups.

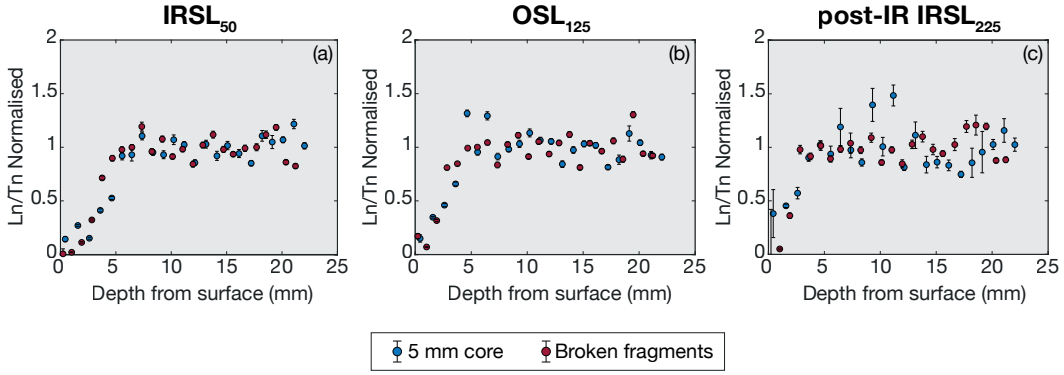

Figure 6: Comparison between the luminescence profiles for the (a) $IRSL_{50}$, (b) OSL_{125} and (c) post-IR $IRSL_{225}$ signals generated from broken fragments (red) and 5 mm diameter slices (blue). Both were placed in stainless steel cups during measurement. The slices were prepared from cores of Sample GG17-05-01, and the measurement protocol applied was that of Experiment Biii. The errors are derived from the square root of the luminescence counts.

467

468 # 5. Discussion

469

470 *5.1 Filter choice and order of stimulation*

471

472 Following the comparison of detection filters in Section 4.2.2, a sequence which uses the BG39
473 + BG3 blue filter pack for IRSL measurements was deemed more suitable as it potentially
474 allows brighter signals to be measured, and the transmission of this filter pack is better centred
475 on the feldspar emission of 410 nm. The reduction in $IRSL_{50}$ absolute signal counts for the
476 natural samples when comparing the results of applying measurement protocol Ai as opposed
477 to protocol Biii is attributed to a difference in surface area of the stimulated samples- protocol
478 Ai used slices of 10 mm diameter whereas protocol Biii had a combination of both 5 mm
479 diameter slices and broken fragments. Regarding the order of stimulation, Figure 3

480 demonstrates that, for both slice diameters, a measurement protocol where the post-IR $IRSL_{225}$
481 stimulation occurs prior to that of OSL_{125} results in an improvement in the post-IR $IRSL_{225}$
482 signal intensity without greatly reducing the OSL_{125} signal. This is because the results show
483 that a stimulation at 225 °C for 200 s has the ability to deplete an OSL signal, when present.
484 Therefore, for measurement on these samples, a sequence order which has the post-IR $IRSL_{225}$
485 stimulation preceding that of OSL_{125} is more appropriate.
486
487 *5.2 Thermal lag*
488
489 The results showed substantial differences in the TL (Fig. 4) and luminescence decay curves
490 (Fig. 5) observed across experiments and slice diameters, as well as highly scattered
491 luminescence results and variable TL peak positions in natural samples measured using
492 experimental protocol Ai as opposed to those measured using protocol Biii (Fig. 2). Since the
493 Risø reader performance was confirmed (Section 3.4), these variations may be attributable to
494 thermal lag. This occurs when a sample is unable to heat at the same rate as the heater plate,
495 and therefore a delay exists between the temperature of the sample compared to the heater
496 plate. The experiments conducted suggest that the effect of thermal lag is more pronounced in
497 results for 10 mm diameter slices than 5 mm diameter slices, and in the post-IR $IRSL_{225}$ signal
498 as opposed to the $IRSL_{50}$ and OSL_{125} signals. This can be explained by the fact that a better
499 thermal contact is achieved between the heater plate and sample when slices are placed within
500 stainless steel cups. In addition, 10 mm slices resting directly on the carousel as opposed to
501 stainless steel cups are more susceptible to movement during measurement which may affect
502 thermal contact with the heater plate. The movement of slices in the first few measurement
503 steps of a sequence, when the sample is raised by the lift for heating or stimulation, could
504 therefore account for some of the scatter in the 10 mm diameter slices.

505

506 The TL curve results demonstrate that slices subjected to a lower heating rate, and with a
507 smaller diameter in stainless steel cups, heat with conditions more similar to those programmed
508 in the sequence. This is shown by a smaller discrepancy between the theoretical and
509 experimental peak positions of the 110 °C peak. The idea is also supported by the lack of peaks
510 and troughs in the TL curves of slices heated at a higher rate (5 °C s^{-1}). The higher heating rate
511 means that the specific temperatures required to evict unstable charge are either being reached
512 with a delay, not being reached at all or are not held for the necessary amount of time prior to
513 optical stimulation.

514

515 Additional modelling using a general kinetic model for quartz (Bailey, 2001) in the R-package
516 'RLumModel' (Friedrich et al., 2016) confirmed that heating was inconsistent, particularly for
517 the 10 mm slices. Since the 10 mm diameter slice results showed the greatest differences in the
518 modelled and experimental 110 °C peak positions, we sought to better comprehend the thermal
519 conditions that these slices were experiencing. To do this, theoretical quartz TL curves across
520 a range of heating rates, from 0.5 °C s^{-1} to 5 °C s^{-1}, were simulated. The experimental 110 °C
521 peak positions were determined visually. The modelled curves were then compared to the
522 experimental TL curves to find the theoretical curve that corresponded best with the data, the
523 results of which are shown in Figure 7. All four experiments had their 10 mm diameter slices
524 effectively heated at a lower rate than prescribed - Experiments A and D were programmed to
525 have a heating rate of 5 °C s^{-1}, yet the samples' TL curves were more representative of a heating
526 rate of ~3 °C s^{-1}. The same pattern is observed in the slices of Experiments B and C, which
527 were assumed to have a heating rate of 1 °C s^{-1} but, according to the model calculations, were
528 heated at a rate closer to ~0.8 °C s^{-1}. However, these heating rates deduced from the modelling
529 cannot be taken as absolute values, as the kinetic parameters of Bailey (2001) used to model

530 the TL curves were also obtained experimentally and thus may also include an unknown
531 amount of thermal lag. Therefore, the inference drawn about the actual heating rate experienced
532 by the samples by comparison to modelled data might still suffer from an aspect of systematic
533 uncertainty.

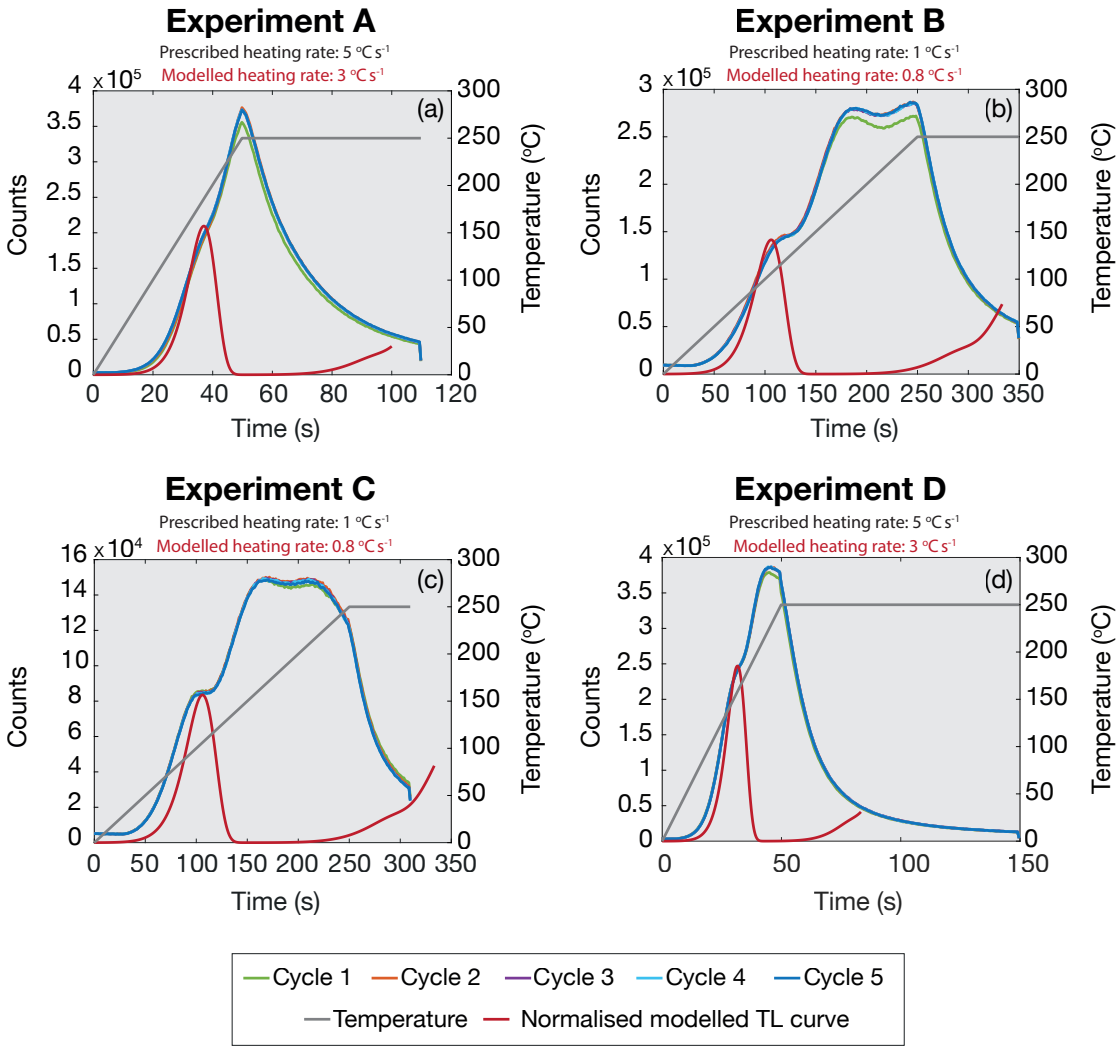

Figure 7: Experimental TL curves across four experiments for 10 mm diameter slices superimposed with the modelled quartz TL curve that best represents the data (red). Experiments A (a) and D (d) measurement results were generated using a prescribed heating rate of 5 °C s^{-1}, but modelling results show that the data are better represented with a heating rate of 3 °C s^{-1}. Experiments B (b) and C (c) measurement results were generated using a prescribed heating rate of 1 °C s^{-1}, but match more closely with modelled TL curves representing a heating rate of 0.8 °C s^{-1}.

534

Evidence of thermal lag is also visible when looking at the post-IR $IRSL_{225}$ luminescence decay curves. As mentioned in Section 4.2.5, there is a "hump" shape observed in the 10 mm diameter slice luminescence decay curves, irrespective of heating rate or isothermal hold duration (Fig. 5). This is indicative of thermal lag because it is assumed that, following the prescribed heating and pre-stimulation isothermal hold, the sample will have reached the desired temperature. Therefore, once the diodes are switched on, the luminescence signal should begin to decay. Instead, we observe the signal continuing to increase even once the diodes have been switched on, which suggests that the sample's temperature was still rising and had not attained a steady value as intended in the sequence programming. This raises the issue of what integration limits to set during data analysis of curves with such shapes. Jain et al. (2007) reported similar luminescence curve shapes for quartz aliquots, and also attributed the initial rise in intensity (and hence overall "hump" shape) to a delay in sample temperature compared to heater plate temperature. In contrast, the 5 mm diameter slices present characteristic luminescence decay shapes once the diodes are switched on, for all experimental conditions. As the two slice diameter types were subjected to identical measurement conditions in each experiment, the considerable improvement between the 10 mm diameter and 5 mm diameter slices' post-IR $IRSL_{225}$ luminescence decay curve results is attributed to improved thermal conductivity when slices are placed in stainless steel cups. The presence of metal between the heater plate and slice allows for better thermal transfer and so the sample is able to heat more rapidly and uniformly than when the slices are sat directly on the carousel.

Whereas our experimental data for both the 5 and 10 mm diameter cores are highly reproducible, the natural TL curves of the 10 mm diameter cores that have been directly placed on the heater plate highly variable between slices (Fig. 2). The cause of the observed TL variability may be due to differences in slice thickness or variable contact between the different

10 mm diameter slices and the heater plate (Fig. 2a-f). In contrast, the 5 mm diameter slices mounted in stainless steel cups exhibit more reproducible behaviour, reflecting uniform contact and heating between measurement cycles.

Overall, the results of the TL curves and luminescence decay curves suggest that while it is beneficial to decrease the heating rate of our samples to reduce the effect of thermal lag, as proposed for the measurement of aliquots by Jain et al. (2007), it is also advised to keep the samples in stainless steel cups when measuring rock slices.

5.3 Exploring a physical process responsible for the scatter in luminescence signals

Comparison of the TL curves measured for the natural signal of GG18-05-01 illustrate considerable variability between 10 mm diameter slices measured using protocol Ai, relative to the 5 mm diameter slices measured using protocol Biii (Fig. 2), indicating that a difference in sample heating may explain the relatively noisy IRSL data obtained (Fig. 1). However, in their study of three K-feldspar samples, Murray et al. (2009) showed that the $IRSL_{50}$ signal of feldspar is insensitive to preheat temperature, making the cause of our observed scatter (Fig. 1) difficult to explain. We conducted a series of further experiments and calculations to try to determine whether our feldspar samples were sensitive to different preheat temperatures and to explain our observations.

Murray et al. (2009) found that the TL trap contribution to the $IRSL_{50}$ signal of feldspar is related to a TL peak at ~410 °C, whilst a lower temperature peak at ~140 °C was present but does not contribute to the $IRSL_{50}$ signal. To investigate this, thermo-optical luminescence (TOL) measurements on a 10 mm diameter slice were undertaken- the temperature of the slice

was heated up to 450 °C, once at a rate of 1 °C $s^{-1}$and then at 5 °C s^{-1}, while quick (0.2 s), periodic IRSL measurements were taken every 2 seconds. This was repeated five times for reproducibility purposes. The results indicated that the 140 °C TL peak does emit an IRSL signal (Fig. S1), that could potentially contribute to the $IRSL_{50}$ or $IRSL_{225}$ signals where preheating has not been sufficient. To explore this, we tested whether the $IRSL_{50}$ and $IRSL_{225}$ signals of our samples were sensitive to different preheat temperatures by modifying the experiment conducted in Figure 3a of Murray et al. (2009). We irradiated our samples with a dose of 57.75 Gy, and then preheated them at temperatures from 70 °C to 340 °C (in 30 °C increments). To mimic our experimental set up, this preheat was applied for either 60 or 100 s, using both heating rates of 1 °C s^{-1} and 5 °C s^{-1}, before measuring the $IRSL_{50}$ and post-IR $IRSL_{225}$ signals. Test dose measurements were made under the same experimental conditions. In agreement with the results of Murray et al. (2009), only minor differences (<5%) in L_x/T_x values were recorded as a function of preheat temperature, with the largest differences occurring following the highest temperature preheats, conditions that our samples were not exposed to during the generation of Fig. 1. Finally, using literature values we calculated the potential thermal depletion of the $IRSL_{50}$ and post-IR $IRSL_{225}$ signals for a 250 °C preheat for 60 s, which is the most stringent possible preheat for samples in this study, and found that no significant signal depletion is anticipated (Fig. 8b). Further calculations were done to try and better understand the effect of inter-slice heating variability, assuming that thermal lag hinders samples from attaining the prescribed preheat temperature (250 °C in this case), but that the degree of thermal lag varies between slices, subsequently affecting the amount of trapped charge released. A value of 46 °C was chosen as an estimate of the maximum thermal lag, taken from the greatest difference in Tn peak position in Figure 2. The trapped charge remaining after holding K-feldspar for 60 s across 100 iterations of randomly generated preheat temperature values from 204 – 250 °C is plotted in Figure 8c-d. For the $IRSL_{50}$ signal, the

610 temperature variation induces up to 3.3 % scatter and up to 0.1 % for the post-IR $IRSL_{225}$ signal
611 (calculations made using the band tail states model (Li and Li, 2013) and kinetic parameters of
612 sample UNIL/NB123 from King et al., 2016). These values are less than the scatter observed

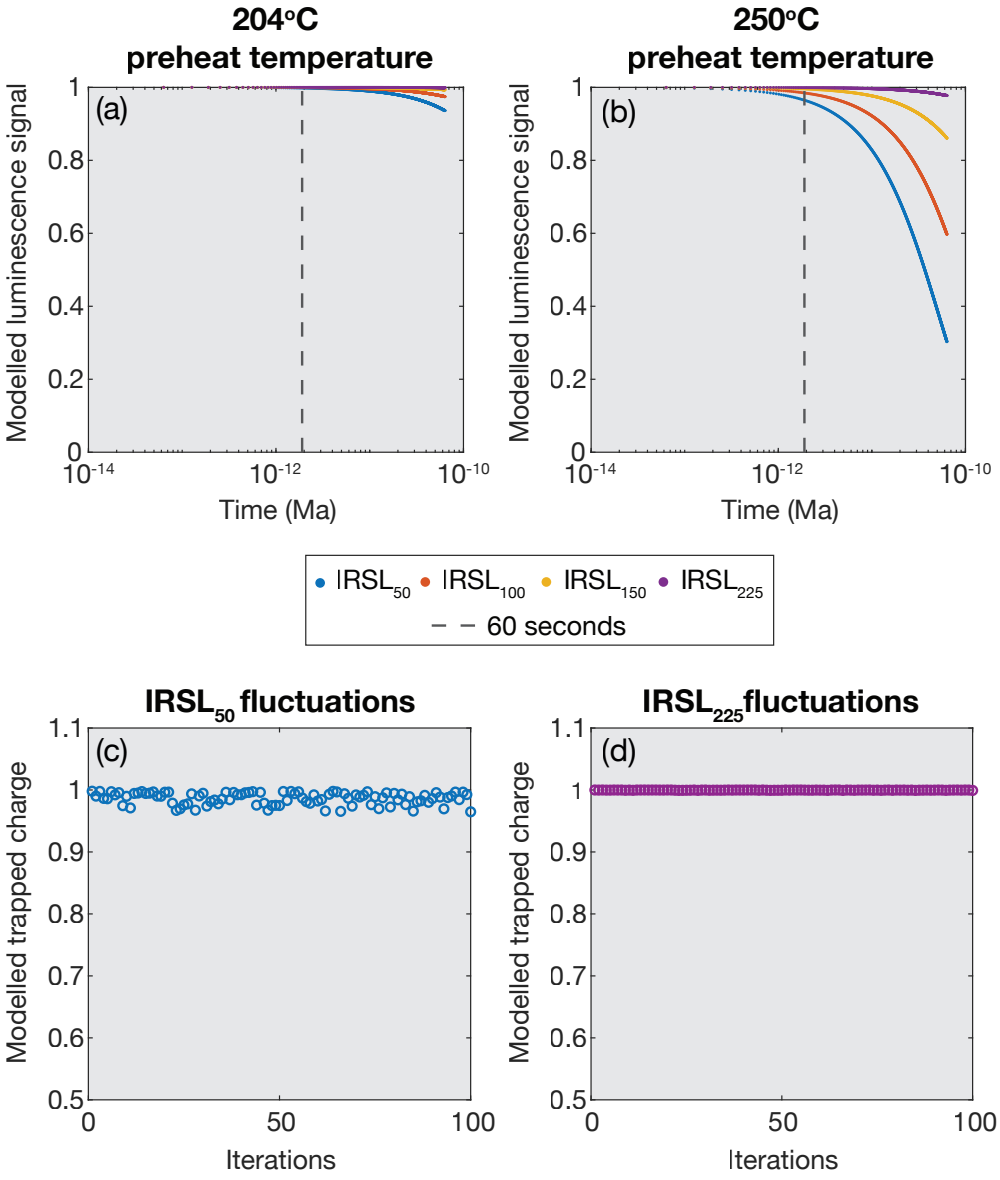

Figure 8: Stimulated isothermal decay at 204 °C (a) and 250 °C (b) for 2000 s using the band tail states model (Li and Li, 2013) and kinetic parameters for sample UNIL/NB123 from King et al., 2015. Depletion after 60 s of holding is marked on the figure. The trapped charge remaining after holding for 60 s across 100 iterations for randomly generated preheat values from 204-250 °C is shown for the $IRSL_{50}$ (c) and post-IR $IRSL_{225}$ (d) signals.

in the luminescence depth profiles of Experiment Ai in Figure 1 and cannot explain what is observed.

On the basis of these results, and in agreement with the data of Murray et al. (2009), it is difficult to reconcile our observations that differences in sample thermal treatment (Fig. 2) is related to increased scatter of the IRSL data (Fig. 1). Nonetheless, we observe that sample slices that have experienced different thermal treatments produce luminescence bleaching profiles with more scatter (Fig. 2). Furthermore, IRSL signal decay differs between 10 mm diameter slices and 5 mm diameter slices of the same samples (Fig. 5), which TL data indicate have experienced different heating conditions (Fig. 4), supporting the notion that the presence of thermal lag must impact the IRSL emission in some way by reducing signal efficiency due to reduced thermal assistance (cf. Hütt, 1988). Since feldspar is known to be highly thermally sensitive (e.g. Duller and Wintle, 1991), it is unsurprising that the $IRSL_{50}$ and post-IR $IRSL_{225}$ luminescence profiles demonstrate a greater improvement in noise reduction than that of OSL_{125} in Figure 1. One potential source of the scatter may lie in the temperature dependence of the infrared stimulated luminescence of feldspars (e.g. Duller and Bøtter-Jensen, 1993; Poolton et al., 2002; Buylaert et al., 2009), and hence its sensitivity to the measurement temperature which might not be consistent across one slice or from slice to slice, although this is not sufficient to fully account for the observed scatter and would only partly contribute.

Whilst the physical process remains unclear, our data demonstrate that protocol modifications, aimed at reducing variations in heating, result in less heterogeneous data (Fig. 1). As all the cores used in the measurement of the natural signal of GG18-05-01 are taken from the same sample with the same exposure history, lithological variations cannot account for this improvement (Fig. 1). Although variation in rates of anomalous fading or thermal stability

could be considered as potential candidates for explaining variance in natural signals of the same sample, Lehmann et al. (2019) have demonstrated the effect of fading to be secondary to bleaching and Riedesel et al. (2019) have shown that the kinetic parameters of chemically different feldspars are similar. Finally, although differences in thermal treatment do not appear to affect subsequent IRSL emissions, TL plots remain useful in allowing the quantification of the degree of thermal lag that the samples are potentially experiencing, which can be done through calculating discrepancies in the experimental and modelled 110 °C peak positions.

6. Implications for OSL rock surface dating

The difference between luminescence profiles with depth (Fig. 1) measured using the protocols of Experiment Ai and Experiment Biii renders it immediately clear that applying the Experiment Biii protocol considerably reduces noise in the data, particularly for the $IRSL_{50}$ and post-IR $IRSL_{225}$ results. This improvement is supported by the TL signals (Fig. 2) and χ^2 values. Core diameters can be chosen depending on the application of the study and lithology of the sample material.

The results from investigating the effect of slice diameter (Section 4.2.6, Fig. 6) imply that slice diameter is inconsequential to the results, and that the predominant factor is the placement of all rock slices in stainless steel cups. Both diameters used in this study (5 or 10 mm) have their advantages. 5 mm diameter cores leave behind a smaller hole in the host rock, and so are potentially more suitable for archaeological studies that prefer to inflict minimal damage to the original material. However, their small diameter results in increased fragility and they are consequently more prone to breakage during sample preparation - namely coring and slicing. The small size of their slices also makes it challenging to accurately measure each slice's

individual thicknesses, affecting depth reconstructions. In comparison, 10 mm diameter cores are more robust during sample preparation and have slice thicknesses which are easier to accurately measure. For heterogeneous lithologies, taking larger diameter cores is also advantageous as this reduces the effect of spatial variations on a sample's measurement reproducibly (Meyer et al., 2019). Each slice can subsequently be broken into several fragments which can be measured separately to build a more comprehensive sample luminescence profile with depth.

6.1 Fit with surface exposure dating model

Data from OSL surface exposure dating measurements can be fitted with a double exponential model that describes the time and depth dependent bleaching of minerals in rock surface dating (Sohbati et al., 2011):

$$\frac{Lx}{Tx}(x,t) = L_0 e^{-\overline{\sigma\varphi_0}te^{-\mu x}} \quad (1)$$

where $\frac{Lx}{Tx}$ is the normalised luminescence signal measured at depth x (mm) after exposure time t (s). L_0 is the maximum luminescence signal intensity at saturation and assumed to have been constant at all depths prior to daylight exposure. μ (cm^{-1}) represents the light attenuation factor and $\overline{\sigma\varphi_0}$ (s^{-1}) represents the decay rate of the luminescence signal at the bedrock surface. The decay rate is assumed to be regionally uniform and is composed of the product of the photoionisation cross section, σ (cm^2) and the photon flux, φ_0($cm^{-2}s^{-1}$).

The biggest challenge currently faced by surface exposure dating is the need to constrain $\overline{\sigma\varphi_0}$ and μ, as it is impossible to calculate an exposure age otherwise. These parameters have been

688 shown to vary greatly across different lithologies, minerals and locations (e.g. Sohbati et al.,
689 2012; Lehmann et al., 2018; Ou et al., 2018). One method of determining the values of these
690 parameters is by local calibration from the luminescence profiles of independently known
691 exposure age samples. The results can then be fed into the model to calculate unknown
692 exposure ages, provided that the calibration and unknown samples are from the same region
693 and lithology. Calibration surfaces can be found from a number of different sources - including
694 historical records (Lehmann et al., 2018), road cut outcrops (Sohbati et al., 2012a) or the
695 creation of a freshly exposed surface that can be resampled at a later date (Gliganic et al., 2019).
696 To assess the implications of using different protocols on OSL surface exposure dating
697 calculations, the latter calibration method was applied using calibration samples subjected to
698 two different protocols. As mentioned in Section 3.1, a surface of unknown exposure age was
699 sampled (GG17-05-01) and then a year later, an additional sample was taken (GG18-05-01)
700 from the freshly exposed surface that had been created the previous year (342 d exposure age).
701 Two luminescence profiles with depth were made for both GG17-05-01 and GG18-05-01 - one
702 using the Experiment Ai protocol, with slices resting directly on the carousel, and the other
703 using that of Experiment Biii, with a combination of 5 mm diameter slices and broken slices
704 in the stainless steel cups. All luminescence profiles were made using at least 3 cores.
705
706 Using the two separate luminescence profiles for GG18-05-01, in combination with Eq. (1)
707 and fixing a known exposure time (t) of 0.936 a, we were able to invert for $\overline{\sigma\varphi_0}$ and μ values
708 across all three signals. We then inverted for their respective protocol GG17-05-01
709 luminescence profile, but this time fixing the $\overline{\sigma\varphi_0}$ and μ values previously determined to
710 calculate exposure ages. The inversions were done using a modified code from Lehmann et al.
711 (2019), with 1 x 10^4 iterations to invert for the unknown parameters and 1 x 10^7 iterations for

712 the exposure age. The results of these inversions are summarised in Table 5, with additional
713 detail in Table S7.

Protocol applied	Experiment Ai			Experiment Biii		
	μ (mm^{-1})	$\overline{\sigma\varphi_0}$ (a^{-1})	Exposure age (a)	μ (mm^{-1})	$\overline{\sigma\varphi_0}$ (a^{-1})	Exposure age (a)
$IRSL_{50}$	2.16	404.32	2.15 ± 0.76	1.19	12.65	2.94 ± 0.25
OSL_{125}	1.68	23.06	0.67 ± 0.11	1.70	10.17	3.36 ± 0.65
post-IR $IRSL_{225}$	2.34	12.65	6.48 ± 1.06	1.60	4.90	3.42 ± 0.63

714 **Table 5:** Results from fitting Equation 1 to luminescence depth profiles subjected to two different
715 protocols - Experiment Ai and Experiment Biii. The $\overline{\sigma\varphi_0}$ and μ values were initially constrained by fixing *t*
716 from a calibration sample, and once generated, the parameters were then used to calculate *t* for an
717 unknown exposure age surface. Experiment Ai involved 10 mm diameter slices resting directly on the
718 carousel. Experiment Biii had a combination of 5 mm diameter slices and broken fragments sat in stainless
719 steel cups on the carousel. The errors on the exposure age are 1σ.

720 The exposure ages calculated using the improved protocol in Experiment Biii all lie within 1σ
721 uncertainty of each other, with more precise OSL_{125} and post-IR $IRSL_{225}$ exposure times. We
722 also observe $\overline{\sigma\varphi_0}$ and μ values within similar orders of magnitude. In contrast, the exposure
723 age results from using the protocol of Experiment Ai are more widespread, less precise and
724 disagree at 2σ. These results highlight the importance of using an appropriate measurement
725 protocol. Furthermore, if the $\overline{\sigma\varphi_0}$ and μ calibration values from Experiment Biii are used to
726 invert the bleaching profile of sample GG17-05-01 measured using the protocol of Experiment
727 Ai, the ages are significantly overestimated, illustrating that it is essential to use the same
728 measurement protocol for both calibration samples and measurement samples.
729
730 *6.2 Recommendations for future OSL rock surface dating protocols*
731

As a result of the experiments in this study, it is recommended that a low heating rate and a long isothermal hold (in this case 1 °C s^{-1} and 100 s respectively) are used (cf. Jenkins et al., 2018) to allow the slices ample time to reach the desired temperature. Furthermore, all samples should be placed in metal cups to improve thermal conductivity between the sample and heater plate, and for these samples it is advantageous to have a sequence in which the post-IR $IRSL_{225}$ stimulation occurs prior to that of OSL_{125}. However, as with all luminescence studies, it is the responsibility of the luminescence practitioner to optimise their measurement protocol for their specific aims and samples.

7. Conclusion

The results from this study show the influence of sample temperature on OSL surface exposure dating measurements, as well as potential implications for age calculations if an unsuitable protocol is used. It is usually assumed that samples heat to the temperature dictated by the measurement protocol. Here, however, we demonstrate that for 10 mm diameter rock slices placed directly on the reader carousel, this may not be the case. This thermal lag can result in anomalously high or low luminescence values, producing noisy luminescence profiles with depth, but the source of this scatter remains unclear. Since luminescence profiles with depth are instrumental to inverting for exposure ages, a noisy profile can affect age calculation. To minimise the effect of thermal lag, it is recommended to increase the isothermal holding time while decreasing the heating rate in the measurement protocol, and that all samples are placed in metal cups. These adjustments allow for the sample to heat at the desired rate and in a uniform manner.

6. Acknowledgements

This work was supported by the Swiss Government Excellence Scholarship (Award number 2017.1136). The authors would like to thank S. Vivero Andrade, D. Rech, C. Bouscary, A. Ballu, L. Malatesta and G. Prasicek for fieldwork support, L. Bossin, R. Biswas and C. Schmidt for laboratory support and stimulating discussions.

7. References

Aitken, M.J., 1985. Thermoluminescence Dating. Studies in Archaeological Science.

Aitken, M.J., 1998. An Introduction to Optical Dating: The Dating of Quaternary Sediments by the Use of Photon-Stimulated Luminescence. Oxford Science Publication.

Bailey, R.M., 2001. Towards a general kinetic model for optically and thermally stimulated luminescence of quartz. Radiation Measurements, 33, 17-45.

Bøtter-Jensen, L., Thomsen, K.J., Jain, M., 2010. Review of optically stimulated luminescence (OSL) instrumental developments for retrospective dosimetry. Radiation Measurements, 45, 253–257.

Buylaert, J.P., Murray, A.S., Thomsen, K.J., Jain, M., 2009. Testing the potential of an elevated temperature IRSL signal from K-feldspar. Radiation Measurements, 44, 560-565.

780 Chapot, M.S., Sohbati, R., Murray, A.S., Pederson, J.L., Rittenour, T.M., 2012. Constraining
781 the age of rock art by dating a rockfall event using sediment and rock-surface luminescence
782 dating techniques. Quaternary Geochronology, 13, 18-25.
783
784 Drury, M.J., 1987. Thermal diffusivity of some crystalline rocks. Geothermics, 16, 105-115.
785
786 Duller, G.A.T., Wintle, A.G., 1991. On infrared stimulated luminescence at elevated
787 temperatures. Nuclear Tracks and Radiation Measurements, 18, 379-384.
788
789 Duller, G.A.T., Bøtter-Jensen, L., 1993. Luminescence from potassium feldspars stimulated by
790 infrared and green light. Radiation Protection Dosimetry, 47, 683-688.
791
792 Duller, G.A.T., 2015. The Analyst software package for luminescence data: overview and
793 recent improvements. Ancient TL, 33, 35-42.
794
795 Duller, G.A.T., Roberts, H.M., Pinder, R.C., 2020. A method for routinely monitoring the
796 reproducibility of thermal pretreatment prior to optically stimulated luminescence
797 measurements. Radiation Measurements, 130, 106210.
798
799 Feathers, J., More, G.M., Quinteros, P.S., Burkholder, J.E., 2019. IRSL dating of rocks and
800 sediments from desert geoglyphs in coastal Peru. Quaternary Geochronology, 49, 177-183.
801
802 Freiesleben, T., Sohbati, R., Murray, A.S., Jain, M., al Khasawneh, S., Hvidt, S., Jakobsen, B.,
803 2015. Mathematical model quantifies multiple daylight exposure and burial events for rock
804 surfaces using luminescence dating. Radiation Measurements, 81, 16-22.

Friedrich, J., Kreutzer, S., Schmidt, C., 2016. Solving ordinary differential equations to understand luminescence: 'RLumModel', an advanced research tool for simulating luminescence in quartz using R. Quaternary Geochronology, 35, 88-100.

Gliganic, L.A., Meyer, M.C., Sohbati, R., Jain, M., Barrett, S., 2019. OSL surface exposure dating of a lithic quarry in Tibet: Laboratory validation and application. Quaternary Geochronology, 49, 199-204.

Habermann, J., Schilles, T., Kalchgruber, R., Wagner, G.A., 2000. Steps towards surface dating using luminescence. Radiation Measurements, 32, 847- 851.

Huntley, D.J., McMullan, W.G., Godfrey-Smith, D.I., Thewalt, M.L.W., 1989. Time-dependent recombination spectra arising from optical ejection of trapped charges in feldspars. Journal of Luminescence, 44, 41- 46.

Hütt, G., Jaek, I., Tchonka, J., 1988. Optical dating: potassium feldspars optical response stimulation spectra. Quaternary Science Reviews, 7, 381-385.

Jain, M., Bøtter-Jensen, L., Murray, A.S., Essery, R., 2007. A peak structure in isothermal luminescence signals in quartz: origin and implications. Journal of Luminescence, 127, 678-688.

828 Jenkins, G.T.H., Duller, G.A.T., Roberts, H.M., Chiverrell, R.C., Glasser, N.F., 2018. A new
829 approach for luminescence dating glaciofluvial deposits- high precision optical dating of
830 cobbles. Quaternary Science Reviews, 192, 263-273.
831
832 Kars, R.H., Reimann, T., Wallinga, J., 2014. Are feldspar SAR protocols appropriate for post-
833 IR IRSL dating? Quaternary Geochronology, 22, 126-136.
834
835 King, G.E., Herman, F., Lambert, R., Valla, P.G., Guralnik, B., 2016. Multi-OSL-
836 thermochronometry of feldspar. Quaternary Geochronology, 33, 76-87.
837
838 al Khasawneh, S., Murray, A.S., Thomsen, K., Abu-Azizeh, W., Tawawneh, M., 2018. Dating
839 a near eastern desert hunting trap (kite) using rock surface luminescence dating. Archaeological
840 and Anthropological Sciences.
841
842 Laskaris, N., Liritzis, I., 2011. A new mathematical approximation of sunlight attenuation in
843 rocks for surface luminescence dating. Journal of Luminescence, 131, 1874- 1884.
844
845 Lapp, T., Kook, M., Murray, A.S., Thomsen, K.J., Buylaert, J.-P., Jain, M., 2015. A new
846 luminescence detection and stimulation head for the Risø TL/OSL reader. Radiation
847 Measurements, 81, 178-184.
848
849 Lehmann, B., Valla, P.G., King, G.E., Herman, F., 2018. Investigation of OSL surface
850 exposure dating to reconstruct post-LIA glacier fluctuations in the French Alps (Mer de Glace,
851 Mont Blanc massif), Quaternary Geochronology, 44, 64-74.
852

853 Lehmann, B., Herman, F., Valla, P.G., King, G.E., Biswas, R.H., 2019. Evaluating post-glacial
854 bedrock erosion and surface exposure duration by coupling in-situ OSL and ^{10}Be dating. Earth
855 Surface Dynamics, 7, 633-662.
856
857 Lehmann, B., Herman, F., Valla, P.G., King, G.E., Biswas, R.H., Ivy-Ochs, S., Steinemann,
858 O., Christl, M., 2020. Postglacial erosion of bedrock surfaces and deglaciation timing: New
859 insights from the Mont Blanc massif (Western Alps). Geology, 48(2), 139-144/
860
861 Li, B., Li, S.H., 2013. The effect of band-tail states on the thermal stability of the infrared
862 stimulated luminescence from K-feldspar. Journal of Luminescence, 136, 5-10.
863
864 Liu, J., Cui, F., Murray, A.S., Sohbati, R., Jain, M., Gao, H., Li, W., Li, C., Li, P., Zhou, T.,
865 Chen, J., 2019. Resetting of the luminescence signal in modern riverbed cobbles along the
866 course of the Shiyang River, China. Quaternary Geochronology, 49, 184-190.
867
868 Luo, M., Chen, J., Liu, J., Qin, J., Owen, L.A., Han, F., Yang, H., Wang, H., Zhang, B., Yin,
869 J., Li, Y., 2018. A test of rock surface luminescence dating using glaciofluvial boulders from
870 the Chinese Pamir. Radiation Measurements, 120, 290-297.
871
872 Liritzis, I., 1994. A new dating method by thermoluminscence of carved megalithic stone
873 building. Comptes Rendus Académie des Science Paris, 319 (série II), 603-610.
874
875 Liritzis, I., Vafiadou, A., 2015. Surface luminescence dating of some Egyptian monuments.
876 Journal of Cultural Heritage,16, 134–150.
877

878 Meyer, M.C., Gliganic, L.A., Jain, M., Sohbati, R., Schmidmair, D., 2018. Lithological
879 controls on light penetration into rock surfaces- Implications for OSL and IRSL surface
880 exposure dating. Radiation Measurements, 120, 298-304.
881
882 Murray, A.S., Wintle, A.G., 2000. Luminescence dating of quartz using an improved single
883 aliquot regenerative-dose protocol. Radiation Measurements, 32, 57-73.
884
885 Murray, A.S., Buylaert, J.P., Thomsen, K.J., Jain, M., 2009. The effect of preheating on the
886 IRSL signal from feldspar. Radiation Measurements, 44, 554-559.
887
888 Ou, X.J., Roberts, H.M., Duller, G.A.T., Gunn, M.D., Perkins, W.T., 2018. Attenuation of light
889 in different rock types and implications for rock surface luminescence dating. Radiation
890 Measurements, 120, 305-311.
891
892 Pagonis, V., Kitis, G., Chen, R., 2003. Applicability of the Zimmerman predose model in the
893 thermoluminescence of predosed and annealed synthetic quartz samples. Radiation
894 Measurements, 37, 267-274.
895
896 Polikreti, K., Michael, C., Maniatis, Y., 2002. Authenticating marble sculptures with
897 thermoluminescence. Ancient TL, 20, 11-18.
898
899 Polikreti, K., Michael, C.T., Maniatis, Y., 2003. Thermoluminescence characteristics of marble
900 and dating of freshly excavated marble objects. Radiation Measurements, 37, 87-94.
901

902 Poolton, N.R.J., Ozanyan, K.B., Wallinga, J., Murray, A.S., Bøtter-Jensen, L., 2002. Electrons
903 in feldspar II: a consideration of the influence of conduction band-tail states on luminescence
904 processes. Physics and Chemistry of Minerals, 29, 217-225.
905
906 Rades, E.F., Sohbati, R., Lüthgens, C., Jain, M., Murray, A.S., 2018. First luminescence-depth
907 profiles from boulders from moraine deposits: Insights into glaciation chronology and transport
908 dynamics in Malta valley, Austria. Radiation Measurements, 120, 281-289.
909
910 Reimann, T., Notenboom, P.D., De Schipper, M.A., Wallinga, J., 2015. Testing for sufficient
911 signal resetting during sediment transport using a polymineral multiple-signal luminescence
912 approach. Quaternary Geochronology, 25, 26-36.
913
914 Rhodes, E.J., 2011. Optically stimulated luminescence dating of sediments over the past
915 200,000 years. Annual Review Earth Planetary Sciences, 39, 461-488.
916
917 Richards, M., 1994. Luminescence dating of quartzite from the Diring Yuriakh site. Thesis,
918 Simon Fraser University, August 1994.
919
920 Riedesel, S., King, G.E., Prasad, A.K., Kumar, R., Finch, A.A., Jain, M., 2019. Optical
921 determination of the width of the band-tail states, and the excited and ground state energies of
922 the principal dosimetric trap in feldspar. Radiation Measurements, 125, 40-51.
923
924 Schmidt, C., Friedrich, J., Adamiec, G., Chruścińska, A., Fasoli, M., Kreutzer, S., Martini, M.,
925 Panzeri, L., Polymeris, G.S., Przegiętka, K., Valla, P.G., King, G.E., Sanderson, D.C.W., 2018.

How reproducible are kinetic parameter constraints of quartz luminescence? An interlaboratory comparison for the 110°C TL peak. Radiation Measurements, 110, 14-24.

Simkins, L.M., Simms, A.R., DeWitt, R., 2013. Relative sea level history of Marguerite Bay, Antarctic Peninsula, derived from optically stimulated luminescence dated beach cobbles. Quaternary Science Reviews, 77, 141-155.

Simms, A.R., DeWitt, R., Kouremenos, P., Drewry, A.M., 2011. A new approach to reconstructing sea levels in Antarctica using optically stimulated luminescence of cobble surfaces. Quaternary Geochronology, 6, 50-60.

Simms, A.R., Ivins, E.R., DeWitt, R., Kouremenos, P., Simkins, L.M., 2012. Timing of the most recent Neoglacial advance and retreat in the South Shetland Islands, Antarctic Peninsula: insights from raised beaches and Holocene uplift rates. Quaternary Science Reviews, 47, 41-55.

Sohbati, R., Murray, A.S., Jain, M., Buylaert, J.-P., Thomsen, K., 2011. Investigating the resetting of OSL signals in rock surfaces. Geochronometria, 38(3), 249-258.

Sohbati, R., Murray, A.S., Chapot, M.S., Jain, M., Pederson, J., 2012a. Optically stimulated luminescence (OSL) as a chronometer for surface exposure dating. Journal of Geophysical Research: Solid Earth, 117, B09202.

Sohbati, R., Murray, A.S., Buylaert, J.-P., Almeida, N.A.C., Cunha, P.P., 2012b. Optically stimulated luminescence (OSL) dating of quartzite cobbles from the Tapada do Montinho archaeological site (east-central Portugal). Boreas, 41, 452-462.

Sohbati, R., Murray, A.S., Jain, M., Avner, U, 2015. Age of a prehistoric "Rodedian" cult site constrained by sediment and rock surface dating techniques. Quaternary Geochronology, 30, 90-99.

Sohbati R., Liu, J., Jain, M., Egholm, D., Paris, R., Guralnik, B., 2018. Centennial-to millennia-scale hard rock erosion rates deduced from luminescence-depth profiles. Earth and Planetary Science Letters, 493, 218-230.

Souza, P.E., Sohbati, R., Murray, A.S., Kroon, A., Clemmensen, L.B., Hede, M.U., Nielsen, L., 2019. Luminescence dating of buried cobble surfaces from sandy beach ridges: a case study from Denmark. Boreas.

Theocaris, P.S., Liritzis, I., Galloway, R.B., 1997. Dating of two Hellenic Pyramids by a novel application of thermoluminescence. Journal of Archaeological Science, 24, 399-405.

Appendix

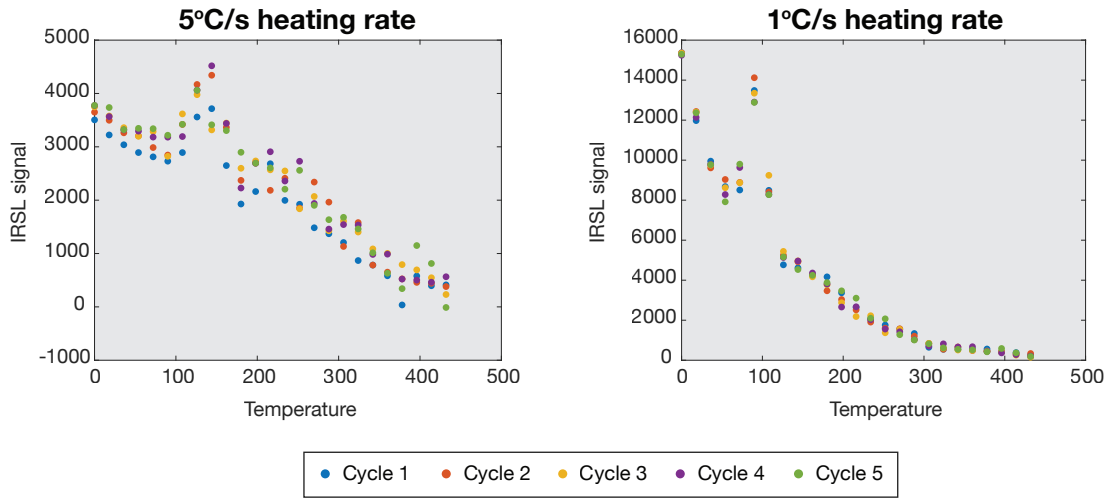

Figure S1: IRSL signal detected during a TOL measurement on a 10 mm diameter slice resting directly on the carousel. The slice was ramped up to 450°C and measured 5 times for reproducibility purposes (termed cycles).

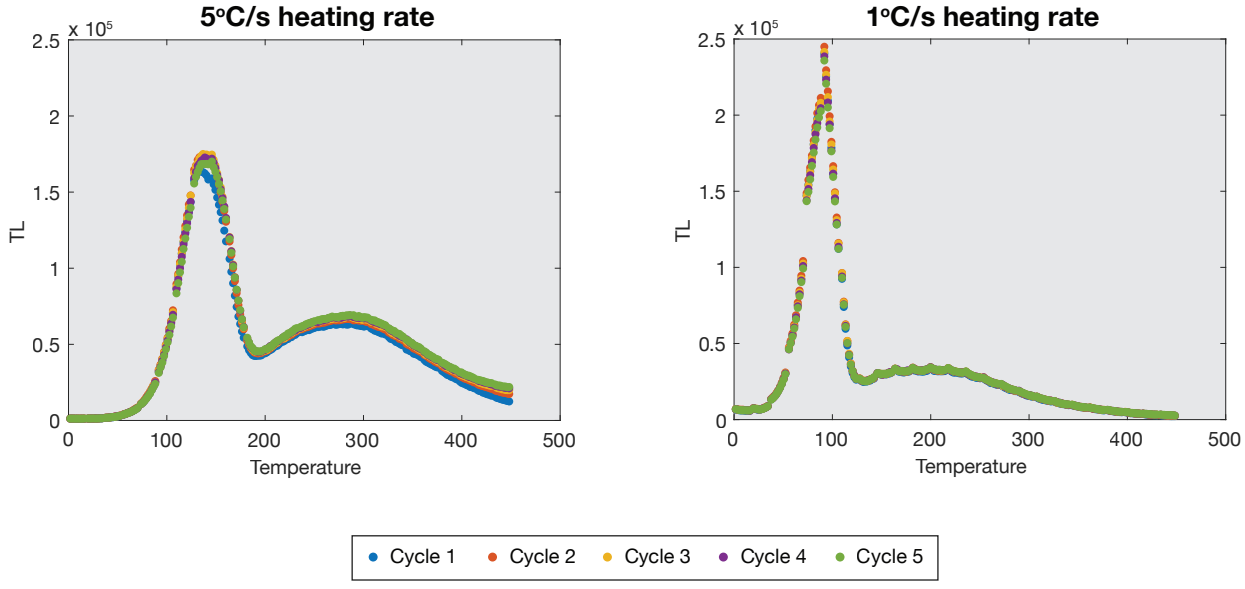

Figure S2: TL curves obtained during the TOL measurement (Section 6) on a 10 mm diameter slice resting directly on the carousel. The slice was ramped up to 450°C and measured 5 times for reproducibility purposes.

Experiment A(i)

Stimulation	Filter	Heating rate ($^{o}C\ s^{-1}$)	Isothermal hold (s)	Signal	Target mineral
Regenerative dose 51.75 Gy					
Preheat to 250°C	U340	5	60		
IRSL at 50°C	U340	5	5	$IRSL_{50}\ L_x$	Feldspar
OSL at 125°C	U340	5	5	$OSL_{125}\ L_x$	Quartz
IRSL at 225°C	U340	5	5	post-IR $IRSL_{225}\ L_x$	Feldspar
Test dose 51.75 Gy					
Preheat to 250°C	U340	5	60		
IRSL at 50°C	U340	5	5	$IRSL_{50}\ T_x$	Feldspar
OSL at 125°C	U340	5	5	$OSL_{125}\ T_x$	Quartz
IRSL at 225°C	U340	5	5	post-IR $IRSL_{225}\ T_x$	Feldspar
Repeat 5 times					

Experiment A(ii)

Stimulation	Filter	Heating rate ($^{o}C\ s^{-1}$)	Isothermal hold (s)	Signal	Target mineral
Regenerative dose 51.75 Gy					
Preheat to 250°C	BG39 + BG3	5	60		
IRSL at 50°C	BG39 + BG3	5	5	$IRSL_{50}\ L_x$	Feldspar
OSL at 125°C	U340	5	5	$OSL_{125}\ L_x$	Quartz
IRSL at 225°C	BG39 + BG3	5	5	post-IR $IRSL_{225}\ L_x$	Feldspar
Test dose 51.75 Gy					
Preheat to 250°C	BG39 + BG3	5	60		
IRSL at 50°C	BG39 + BG3	5	5	$IRSL_{50}\ T_x$	Feldspar
OSL at 125°C	U340	5	5	$OSL_{125}\ T_x$	Quartz
IRSL at 225°C	BG39 + BG3	5	5	post-IR $IRSL_{225}\ T_x$	Feldspar
Repeat 5 times					

Experiment A(iii)

Stimulation	Filter	Heating rate ($^{o}C\ s^{-1}$)	Isothermal hold (s)	Signal	Target mineral
Regenerative dose 51.75 Gy					
Preheat to 250°C	BG39 + BG3	5	60		
IRSL at 50°C	BG39 + BG3	5	5	$IRSL_{50}\ L_x$	Feldspar
IRSL at 225°C	BG39 + BG3	5	5	$OSL_{125}\ L_x$	Quartz
OSL at 125°C	U340	5	5	post-IR $IRSL_{225}\ L_x$	Feldspar
Test dose 51.75 Gy					
Preheat to 250°C	BG39 + BG3	5	60		
IRSL at 50°C	BG39 + BG3	5	5	$IRSL_{50}\ T_x$	Feldspar
IRSL at 225°C	BG39 + BG3	5	5	$OSL_{125}\ T_x$	Quartz
OSL at 125°C	U340	5	5	post-IR $IRSL_{225}\ T_x$	Feldspar

Repeat 5 times

Table S1: Measurement protocol for the three parts of Experiment A.

Experiment B(i)

Stimulation	Filter	Heating rate ($^{o}C\ s^{-1}$)	Isothermal hold (s)	Signal	Target mineral
Regenerative dose 51.75 Gy					
Preheat to 250°C	U340	1	100		
IRSL at 50°C	U340	1	100	$IRSL_{50}\ L_x$	Feldspar
OSL at 125°C	U340	1	100	$OSL_{125}\ L_x$	Quartz
IRSL at 225°C	U340	1	100	post-IR $IRSL_{225}\ L_x$	Feldspar
Test dose 51.75 Gy					
Preheat to 250°C	U340	1	100		
IRSL at 50°C	U340	1	100	$IRSL_{50}\ T_x$	Feldspar
OSL at 125°C	U340	1	100	$OSL_{125}\ T_x$	Quartz
IRSL at 225°C	U340	1	100	post-IR $IRSL_{225}\ T_x$	Feldspar
Repeat 5 times					

Experiment B(ii)

Stimulation	Filter	Heating rate ($^{o}C\ s^{-1}$)	Isothermal hold (s)	Signal	Target mineral
Regenerative dose 51.75 Gy					
Preheat to 250°C	BG39 + BG3	1	100		
IRSL at 50°C	BG39 + BG3	1	100	$IRSL_{50}\ L_x$	Feldspar
OSL at 125°C	U340	1	100	$OSL_{125}\ L_x$	Quartz
IRSL at 225°C	BG39 + BG3	1	100	post-IR $IRSL_{225}\ L_x$	Feldspar
Test dose 51.75 Gy					
Preheat to 250°C	BG39 + BG3	1	100		
IRSL at 50°C	BG39 + BG3	1	100	$IRSL_{50}\ T_x$	Feldspar
OSL at 125°C	U340	1	100	$OSL_{125}\ T_x$	Quartz
IRSL at 225°C	BG39 + BG3	1	100	post-IR $IRSL_{225}\ T_x$	Feldspar
Repeat 5 times					

Experiment B(iii)

Stimulation	Filter	Heating rate ($^{o}C\ s^{-1}$)	Isothermal hold (s)	Signal	Target mineral
Regenerative dose 51.75 Gy					
Preheat to 250°C	BG39 + BG3	1	100		
IRSL at 50°C	BG39 + BG3	1	100	$IRSL_{50}\ L_x$	Feldspar
IRSL at 225°C	BG39 + BG3	1	100	$OSL_{125}\ L_x$	Quartz
OSL at 125°C	U340	1	100	post-IR $IRSL_{225}\ L_x$	Feldspar
Test dose 51.75 Gy					
Preheat to 250°C	BG39 + BG3	1	100		
IRSL at 50°C	BG39 + BG3	1	100	$IRSL_{50}\ T_x$	Feldspar
IRSL at 225°C	BG39 + BG3	1	100	$OSL_{125}\ T_x$	Quartz
OSL at 125°C	U340	1	100	post-IR $IRSL_{225}\ T_x$	Feldspar

	Repeat 5 times

973

974 Table S2: Measurement protocol for the three parts of Experiment B.

Experiment C(i)

Stimulation	Filter	Heating rate ($^{o}C\ s^{-1}$)	Isothermal hold (s)	Signal	Target mineral
Regenerative dose 51.75 Gy					
Preheat to 250^{o}C	U340	1	60		
IRSL at 50^{o}C	U340	1	5	$IRSL_{50}$ L_x	Feldspar
OSL at 125^{o}C	U340	1	5	OSL_{125} L_x	Quartz
IRSL at 225^{o}C	U340	1	5	post-IR $IRSL_{225}$ L_x	Feldspar
Test dose 51.75 Gy					
Preheat to 250^{o}C	U340	1	60		
IRSL at 50^{o}C	U340	1	5	$IRSL_{50}$ T_x	Feldspar
OSL at 125^{o}C	U340	1	5	OSL_{125} T_x	Quartz
IRSL at 225^{o}C	U340	1	5	post-IR $IRSL_{225}$ T_x	Feldspar
Repeat 5 times					

Experiment C(ii)

Stimulation	Filter	Heating rate ($^{o}C\ s^{-1}$)	Isothermal hold (s)	Signal	Target mineral
Regenerative dose 51.75 Gy					
Preheat to 250^{o}C	BG39 + BG3	1	60		
IRSL at 50^{o}C	BG39 + BG3	1	5	$IRSL_{50}$ L_x	Feldspar
OSL at 125^{o}C	U340	1	5	OSL_{125} L_x	Quartz
IRSL at 225^{o}C	BG39 + BG3	1	5	post-IR $IRSL_{225}$ L_x	Feldspar
Test dose 51.75 Gy					
Preheat to 250^{o}C	BG39 + BG3	1	60		
IRSL at 50^{o}C	BG39 + BG3	1	5	$IRSL_{50}$ T_x	Feldspar
OSL at 125^{o}C	U340	1	5	OSL_{125} T_x	Quartz
IRSL at 225^{o}C	BG39 + BG3	1	5	post-IR $IRSL_{225}$ T_x	Feldspar
Repeat 5 times					

Experiment C(iii)

Stimulation	Filter	Heating rate ($^{o}C\ s^{-1}$)	Isothermal hold (s)	Signal	Target mineral
Regenerative dose 51.75 Gy					
Preheat to 250^{o}C	BG39 + BG3	1	60		
IRSL at 50^{o}C	BG39 + BG3	1	5	$IRSL_{50}$ L_x	Feldspar
IRSL at 225^{o}C	BG39 + BG3	1	5	OSL_{125} L_x	Quartz
OSL at 125^{o}C	U340	1	5	post-IR $IRSL_{225}$ L_x	Feldspar
Test dose 51.75 Gy					
Preheat to 250^{o}C	BG39 + BG3	1	60		
IRSL at 50^{o}C	BG39 + BG3	1	5	$IRSL_{50}$ T_x	Feldspar
IRSL at 225^{o}C	BG39 + BG3	1	5	OSL_{125} T_x	Quartz
OSL at 125^{o}C	U340	1	5	post-IR $IRSL_{225}$ T_x	Feldspar

	Repeat 5 times

975

976 Table S3: Measurement protocol for the three parts of Experiment C.

Experiment D(i)

Stimulation	Filter	Heating rate (°C s^{-1})	Isothermal hold (s)	Signal	Target mineral
Regenerative dose 51.75 Gy					
Preheat to 250°C	U340	5	100		
IRSL at 50°C	U340	5	100	$IRSL_{50}$ L_x	Feldspar
OSL at 125°C	U340	5	100	OSL_{125} L_x	Quartz
IRSL at 225°C	U340	5	100	post-IR $IRSL_{225}$ L_x	Feldspar
Test dose 51.75 Gy					
Preheat to 250°C	U340	5	100		
IRSL at 50°C	U340	5	100	$IRSL_{50}$ T_x	Feldspar
OSL at 125°C	U340	5	100	OSL_{125} T_x	Quartz
IRSL at 225°C	U340	5	100	post-IR $IRSL_{225}$ T_x	Feldspar
Repeat 5 times					

Experiment D(ii)

Stimulation	Filter	Heating rate (°C s^{-1})	Isothermal hold (s)	Signal	Target mineral
Regenerative dose 51.75 Gy					
Preheat to 250°C	BG39 + BG3	5	100		
IRSL at 50°C	BG39 + BG3	5	100	$IRSL_{50}$ L_x	Feldspar
OSL at 125°C	U340	5	100	OSL_{125} L_x	Quartz
IRSL at 225°C	BG39 + BG3	5	100	post-IR $IRSL_{225}$ L_x	Feldspar
Test dose 51.75 Gy					
Preheat to 250°C	BG39 + BG3	5	100		
IRSL at 50°C	BG39 + BG3	5	100	$IRSL_{50}$ T_x	Feldspar
OSL at 125°C	U340	5	100	OSL_{125} T_x	Quartz
IRSL at 225°C	BG39 + BG3	5	100	post-IR $IRSL_{225}$ T_x	Feldspar
Repeat 5 times					

Experiment D(iii)

Stimulation	Filter	Heating rate (°C s^{-1})	Isothermal hold (s)	Signal	Target mineral
Regenerative dose 51.75 Gy					
Preheat to 250°C	BG39 + BG3	5	100		
IRSL at 50°C	BG39 + BG3	5	100	$IRSL_{50}$ L_x	Feldspar
IRSL at 225°C	BG39 + BG3	5	100	OSL_{125} L_x	Quartz
OSL at 125°C	U340	5	100	post-IR $IRSL_{225}$ L_x	Feldspar
Test dose 51.75 Gy					
Preheat to 250°C	BG39 + BG3	5	100		
IRSL at 50°C	BG39 + BG3	5	100	$IRSL_{50}$ T_x	Feldspar
IRSL at 225°C	BG39 + BG3	5	100	OSL_{125} T_x	Quartz
OSL at 125°C	U340	5	100	post-IR $IRSL_{225}$ T_x	Feldspar

Repeat 5 times

Table S4: Measurement protocol for the three parts of Experiment D.

Protocol applied	Experiment Ai			Experiment Biii		
	$IRSL_{50}$					
	μ (mm^{-1})	$\overline{\sigma\varphi_0}$ (a^{-1})	Exposure time (a)	μ (mm^{-1})	$\overline{\sigma\varphi_0}$ (a^{-1})	Exposure time (a)
Median	2.16	404.32	2.15	1.19	12.65	2.94
+1 SD	2.94	5903.80	2.91	1.91	57.44	3.18
-1 SD	1.20	54.21	1.77	1.00	4.61	2.69
+ 2SD	3.32	11540.93	3.29	2.64	260.91	3.35
- 2SD	0.81	7.25	1.39	0.64	2.78	2.45
	OSL_{125}					
	μ (mm^{-1})	$\overline{\sigma\varphi_0}$ (a^{-1})	Exposure time (a)	μ (mm^{-1})	$\overline{\sigma\varphi_0}$ (a^{-1})	Exposure time (a)
Median	1.68	23.06	0.67	1.70	10.17	3.36
+1 SD	2.79	568.83	0.76	2.81	43.95	4.01
-1 SD	0.94	4.64	0.56	1.34	4.89	3.03
+ 2SD	3.35	2825.35	0.78	3.36	91.39	4.33
- 2SD	0.75	2.72	0.47	0.97	2.35	2.38
	post-IR $IRSL_{125}$					
	μ (mm^{-1})	$\overline{\sigma\varphi_0}$ (a^{-1})	Exposure time (a)	μ (mm^{-1})	$\overline{\sigma\varphi_0}$ (a^{-1})	Exposure time (a)
Median	2.34	1.14	6.48	1.60	4.90	3.42
+1 SD	3.51	26.21	7.53	2.75	9.84	4.05
-1 SD	1.17	0.05	5.42	1.02	2.44	2.80
+ 2SD	3.71	125.89	8.23	3.52	39.64	4.45
- 2SD	0.39	0.00	4.37	0.83	1.22	2.39

Table S7: Unknown parameter and exposure age results from the modelling.

$IRSL_{50}$
Position 1 (10 mm diameter slice)

	Experiment Bi- U430 filter			Experiment Bii- BG39 + BG3			Experiment Di- U430 filter			Experiment Dii- BG39 + BG3		
	Signal	BG	Lx	Signal	BG	Lx	Signal	BG	Lx	Signal	BG	Lx
Cycle 1	6.5E+04	1.4E+03	6.3E+04	5.6E+04	2.6E+03	5.4E+04	3.8E+04	8.9E+02	3.7E+04	4.0E+04	2.5E+03	3.8E+04
Cycle 2	6.2E+04	1.3E+03	6.1E+04	5.6E+04	2.6E+03	5.4E+04	2.9E+04	7.8E+02	2.8E+04	4.0E+04	2.5E+03	3.8E+04
Cycle 3	6.1E+04	1.3E+03	6.0E+04	5.6E+04	2.6E+03	5.3E+04	2.8E+04	7.7E+02	2.7E+04	4.0E+04	2.5E+03	3.8E+04
Cycle 4	6.1E+04	1.3E+03	6.0E+04	5.6E+04	2.6E+03	5.3E+04	2.8E+04	7.6E+02	2.7E+04	4.0E+04	2.5E+03	3.8E+04
Cycle 5	6.1E+04	1.3E+03	5.9E+04	5.6E+04	2.5E+03	5.3E+04	2.7E+04	7.3E+02	2.6E+04	4.0E+04	2.5E+03	3.7E+04
Average intensity			6.1E+04			5.3E+04			2.9E+04			3.8E+04

post-IR $IRSL_{225}$
Position 1 (10 mm diameter slice)

	Experiment Bi- U430 filter			Experiment Bii- BG39 + BG3			Experiment Di- U430 filter			Experiment Dii- BG39 + BG3		
	Signal	BG	Lx	Signal	BG	Lx	Signal	BG	Lx	Signal	BG	Lx
Cycle 1	6.0E+03	5.2E+03	9.1E+02	3.1E+04	2.8E+04	3.6E+03	5.5E+03	4.0E+03	1.5E+03	3.4E+04	2.9E+04	5.5E+03
Cycle 2	5.2E+03	4.5E+03	6.5E+02	3.1E+04	2.7E+04	3.4E+03	3.7E+03	2.7E+03	9.5E+02	3.4E+04	2.9E+04	5.2E+03
Cycle 3	5.4E+03	4.4E+03	9.9E+02	3.1E+04	2.7E+04	3.3E+03	3.5E+03	2.5E+03	9.4E+02	3.4E+04	2.9E+04	5.2E+03
Cycle 4	5.1E+03	4.2E+03	8.6E+02	3.0E+04	2.7E+04	3.2E+03	3.4E+03	2.5E+03	9.0E+02	3.4E+04	2.9E+04	5.3E+03
Cycle 5	4.9E+03	4.3E+03	6.5E+02	3.1E+04	2.7E+04	3.7E+03	3.4E+03	2.4E+03	1.0E+03	3.4E+04	2.9E+04	5.1E+03
Average intensity			8.1E+02			3.5E+03			1.1E+03			5.3E+03

Table S5: Lx signal intensities for a 10 mm diameter slice across parts (i) and (ii) of Experiments B and D for both the $IRSL_{50}$ and post-IR $IRSL_{225}$ signals.

$IRSL_{50}$
Position 11 (5 mm diameter slice)

	Experiment Bi- U430 filter			Experiment Bii- BG39 + BG3			Experiment Di- U430 filter			Experiment Dii- BG39 + BG3		
	Signal	BG	Lx	Signal	BG	Lx	Signal	BG	Lx	Signal	BG	Lx
Cycle 1	3.5E+03	2.2E+02	3.3E+03	9.5E+03	2.8E+03	6.7E+03	1.4E+03	2.8E+02	1.1E+03	5.9E+03	2.5E+03	3.4E+03
Cycle 2	3.4E+03	2.4E+02	3.2E+03	9.7E+03	2.9E+03	6.8E+03	1.3E+03	2.6E+02	1.0E+03	5.8E+03	2.5E+03	3.3E+03
Cycle 3	3.4E+03	2.1E+02	3.2E+03	9.5E+03	2.9E+03	6.6E+03	1.2E+03	2.7E+02	9.4E+02	5.8E+03	2.6E+03	3.2E+03
Cycle 4	3.2E+03	1.8E+02	3.0E+03	9.3E+03	2.8E+03	6.5E+03	1.3E+03	2.8E+02	9.8E+02	5.9E+03	2.5E+03	3.4E+03
Cycle 5	3.0E+03	2.1E+02	2.8E+03	9.2E+03	2.8E+03	6.4E+03	1.1E+03	2.6E+02	8.9E+02	5.7E+03	2.5E+03	3.2E+03
Average intensity			3.1E+03			6.6E+03			9.9E+02			3.3E+03

post-IR $IRSL_{225}$
Position 11 (5 mm diameter slice)

	Experiment Bi- U430 filter			Experiment Bii- BG39 + BG3			Experiment Di- U430 filter			Experiment Dii- BG39 + BG3		
	Signal	BG	Lx	Signal	BG	Lx	Signal	BG	Lx	Signal	BG	Lx
Cycle 1	1.4E+03	7.8E+02	6.2E+02	7.8E+03	5.4E+03	2.4E+03	8.3E+02	5.1E+02	3.3E+02	7.4E+03	5.6E+03	1.8E+03
Cycle 2	1.3E+03	7.6E+02	5.3E+02	7.6E+03	5.5E+03	2.2E+03	7.9E+02	4.9E+02	3.0E+02	7.3E+03	5.5E+03	1.8E+03
Cycle 3	1.4E+03	7.6E+02	6.4E+02	7.7E+03	5.5E+03	2.2E+03	7.5E+02	5.3E+02	2.1E+02	7.3E+03	5.4E+03	1.9E+03
Cycle 4	1.4E+03	7.4E+02	6.5E+02	7.7E+03	5.5E+03	2.2E+03	6.9E+02	5.2E+02	1.8E+02	7.2E+03	5.4E+03	1.9E+03
Cycle 5	1.3E+03	7.2E+02	6.0E+02	7.6E+03	5.4E+03	2.2E+03	7.4E+02	5.2E+02	2.2E+02	7.1E+03	5.4E+03	1.7E+03
Average intensity			6.1E+02			2.2E+03			2.5E+02			1.8E+03

Table S6: Lx signal intensities for a 5 mm diameter slice across parts (i) and (ii) of Experiments B and D for both the $IRSL_{50}$ and post-IR $IRSL_{225}$ signals.